Investigating Electrical and Photoconductive Properties of Aluminum Nitride Nanowire (AlNNW) Based Ultraviolet (UV) Photodetector

A thesis submitted to the
Graduate School of Natural and Applied Sciences

by

Yassir Abdullahi Ali

in partial fulfillment for the
degree of Master of Science

in

Electronics and Computer Engineering

This is to certify that we have read this thesis and that in our opinion it is fully adequate, in scope and quality, as a thesis for the degree of Master of Science in Electronics and Computer Engineering.

APPROVED BY:

Prof. Kaşif Teker ....
(Thesis Advisor)

Assist. Prof. İhsan Çiçek ....

Assoc. Prof. Tansal Güçlüoğlu ....

This is to confirm that this thesis complies with all the standards set by the Graduate School of Natural and Applied Sciences of İstanbul Şehir University:

DATE OF APPROVAL:

SEAL/SIGNATURE:

Declaration of Authorship

I, Yassir Abdullahi Ali, declare that this thesis titled, 'Investigating Electrical and Photoconductive Properties of Aluminum Nitride Nanowire (AlNNW) Based Ultraviolet (UV) Photodetector' and the work presented in it are my own. I confirm that:

- This work was done wholly or mainly while in candidature for a research degree at this University.
- Where any part of this thesis has previously been submitted for a degree or any other qualification at this University or any other institution, this has been clearly stated.
- Where I have consulted the published work of others, this is always clearly attributed.
- Where I have quoted from the work of others, the source is always given. With the exception of such quotations, this thesis is entirely my own work.
- I have acknowledged all main sources of help.
- Where the thesis is based on work done by myself jointly with others, I have made clear exactly what was done by others and what I have contributed myself.

Signed: 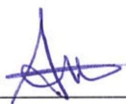

Date: 23-01-2019

"There is plenty of room at the bottom"

Richard Feynman

Investigating Electrical and Photoconductive Properties of Aluminum Nitride Nanowire (AlNNW) Based Ultraviolet (UV) Photodetector

Yassir Abdullahi Ali

Abstract

One-dimensional nanostructured wide bandgap (WBG) semiconductor nanomaterials (typically E_g 3 eV − 6 eV) are good candidates as building blocks for photosensitive device applications such as UV photodetectors, phototransistors, and photodiodes. Furthermore, high UV light sensitivity, small sizes, quick response times, low power consumption, and high efficiency are the most important features of nanodevices for new and superior photonic applications. AlN nanostructures, an important III-nitride WBG semiconductor, have attracted significant attention due to its large direct bandgap (6.28 eV), low electron affinity, high thermal conductivity, high melting point (above 2300 °C), and chemical stability. Despite its intrinsic superior properties, challenges in synthesis of defect free and uniform morphology AlN nanostructures persist, thereby limiting the number of electronic and photonic device studies.

This work presents the fabrication of a flexible ultraviolet (UV) photodetector from free-standing catalyst-free grown AlN nanowire (AlNNW) films via a direct transfer method through a very low-cost non-lithographic fabrication scheme. The device has demonstrated a quick photoresponse rise and decay times of 0.27 s and 0.41 s to the deep-UV light illumination, respectively. The photocurrent measurements have been conducted for bias voltages ranging from 1V to 20V. In fact, the flexible AlNNW photodetector is very sensitive to the UV illumination even at low bias voltages (as low as 1V) indicating very high sensitivity and capability of operating at low voltages. Moreover, the photocurrent rapidly dropped to dark current values upon turning off the UV light, suggesting the absence of defect-related traps. Consequently, the facile fabrication scheme is very cost-effective, readily scalable; and offers broad integration capabilities in various flexible photonic and electronic applications including wearable devices.

Keywords: Photoconductivity, Flexible cost-effective UV sensors, Wide bandgap semiconductors, Deep-UV photodetectors, AlN nanowire film, low voltage operation, Non-lithographic fabrication, Photoresponse, Rise time, Decay time, Responsivity.

Alüminyum Nitrür Nanotel (UV) Esaslı Ultraviyole (UV) Fotodetektörün Elektriksel ve Foto Iletkenlik Özelliklerinin Araştırılması

Yassir Abdullahi Ali

Öz

Geniş bant aralıklı (WBG, tipik olarak 3 eV 6eV arasında) tek boyutlu nanoyapılı yarı iletken malzemeler UV fotodetektörler, fototransistörler ve fotodiyodlar gibi ışığa duyarlı cihaz uygulamaları için yapı taşları olarak kullanılabilecek iyi adaylardır. Ayrıca, yüksek UV ışık hassasiyet, küçük boyut, çabuk tepki süresi, düşük güç tüketimi ve yüksek verimlilik, yeni ve üstün fotonik uygulamalarda nano cihazlarda istenilen önemli özelliklerdir. önemli bir III-nitrür grubu WBG yarı iletkeni olan AlN nanoyapılar, büyük doğrudan bant boşluğu (6.28 eV), düşük elektron ilginliği, yüksek termal iletkenliği, yüksek erime noktası (2300 °C yukarısı) ve kimyasal kararlılığı sebebiyle önemli bir ilgi odağı olmuştur. AlN'in içsel üstün özelliklerine rağmen, hatasız ve tek tip morfolojiye sahip AlN nanoyapılarının sentezindeki zorluklar devam etmekte, bu sebeple de elektronik ve fotonik cihaz çalışmalarının sayısı sınırlanmaktadır.
Bu çalışma, çok düşük maliyetli, herhangi bir litografi metoduna gereksinim duyulmayan bir imalat şeması aracılığıyla, doğrudan transfer yöntemi ile serbest duran, katalizör kullanmadan sentezlenmiş AlN nanowire (AlNNW) filmlerinden bir ultraviyole (UV) fotodetektörününü retilmesini sunmaktadır. Cihaz, derin UV ışığa hızlı bir tepki göstererek sırasıyla 0.27 s ve 0.41 s'lik bir tepki ve azalma süreleri göstermiştir. Foto akım ölçümleri 1 V ile 20 V arasında değişen ön gerilimlerde yapılmıştır. Aslında, esnek AlNNW fotodetektör, düşük ön gerilim değerlerinde (1V kadar düşük) bile çok yüksek hassasiyet göstererek hassas UV ışık duyarlılığını ve düşük voltajlarda çalışabilme yeteneğini göstermektedir. Dahası, foto akım, UV ışığı kapatıldıktan sonra karanlık akım değerine hızla düşerek üretilen AlN filimde kusur bulunmadığını göstermektedir. Sonuç olarak, kolay fabrikasyon şeması çok uygun maliyetli, kolayca ölçeklenebilir; ve giyilebilir cihazlar da dahil olmak üzere çeşitli esnek fotonik ve elektronik uygulamalarda geniş entegrasyon imkanı sunmaktadır.

Anahtar Sözcükler: Işıliletkenlik, Esnek uygun maliyetli UV sensör, Geniş bant aralıklı yarıletkenler, Derin UV fotodedektörler, AlN nanotel film, Düşük çalışma gerilimi, Litografisiz imalat, Işık tepkisi, Tepki süresi, Azalma süresi, Fotodedektör kazancı.

I would like to dedicate this work to my parents and siblings for their unwavering support and love.

Acknowledgments

I would like to first extend my sincere gratitude to my thesis advisor and chair of Electrical and Electronic department Prof. Kaşif Teker, for his guidance and mentorship throughout my graduate study and research. His immense knowledge and experience has steered me in the right direction to pursue my career goals.

I am also grateful to my colleagues at Advanced Nano and devices lab; Ali Uzun and Mustafa Akif Yıldım with whom i had the pleasure to learn, work and grow together. I would be remiss if i did not mention my faculty mates at Istanbul Sehir University; Bijan Bibak and Mohamad Shaikh for their constructive criticism of my work.

No one has been more supportive of me throughout my project than my friends. My deep appreciation and thanks goes to; Abdinasir Jimale, Abdelrahman Mahmoud, Ala Mohsen, Irhad Puce, Mutasem Abuzaid, Mohamed Abdulqadir and Nino Ferko who propelled me to be better and do better.

Finally my journey would not be possible without the unconditional support of my family and parents. Their emotional, physical and moral support has kept me focused and inspired.

Contents

Declaration of Authorship ii

Abstract iv

Öz v

Acknowledgments vii

List of Figures x

Abbreviations xii

Physical Constants xiv

Symbols xv

1 Introduction 1
- 1.1 Summary . . . 1
- 1.2 Low dimensional semiconductor materials . . . 2
  - 1.2.1 Ultraviolet light . . . 3
  - 1.2.2 UV detector types . . . 4
    - 1.2.2.1 Photoconductive detectors . . . 5
    - 1.2.2.2 Photovoltaic detectors . . . 6
- 1.3 Materials for UV photodetectors . . . 6
  - 1.3.1 Aluminum Nitride (AlN) . . . 7

2 Experimental details 8
- 2.1 AlNNW Growth . . . 8
- 2.2 NW Characterization . . . 10
  - 2.2.1 Scanning Electron Microscope (SEM) . . . 10
  - 2.2.2 Transmission Electron Microscope (TEM) . . . 13
  - 2.2.3 Raman Spectroscometer . . . 15
- 2.3 Device Fabrication . . . 17
  - 2.3.1 Substrate preparation and cleaning. . . . 18
  - 2.3.2 The deposition of the AlNNWs on the substrate. . . . 18
  - 2.3.3 Masking and the deposition of the Au electrodes on the nanowire network channel. . . . 19
  - 2.3.4 The flexible AlNNW based UV photodetector. . . . 19

3 Photoconductive properties of flexible AlNNW UV photodetector 21
3.1 Introduction . . . 21
3.2 Current - Voltage (I - V) characteristic . . . 22
3.3 Response times . . . 25
3.3.1 Response times at low voltages . . . 25
3.3.2 Response times at high voltages . . . 26
3.3.3 Rise time and decay time . . . 29
3.3.4 Current Responsivity . . . 30
3.4 Performance comparison with other low-dimensional UV photodetectors . 31

4 Conclusion and Future Work 33
4.1 Conclusion . . . 33
4.2 Future Work . . . 34

Bibliography 35

List of Figures

1.1 The commonly used spectral ranges of UV light. 3
1.2 A classification of UV detector types as well as their schematic structure. 5

2.1 MOCVD equipment used for the growth of the nanowires. The lower image depicts the quartz tube inside where the reaction occurs. 9
2.2 SEM (Phenom XL) used to image the nanowires. Its mode of operation is illustrated in the bottom figure. 11
2.3 SEM images of the dense AlNNW films grown catalyst-free at 1100 °C at low magnification. a) 100x b) 300x c) 1100x d) 3000x 12
2.4 SEM images of the AlNNW films at higher magnification. a) 5000x b) 7000x c) 9000x d) 12000x 13
2.5 Electron-atom interaction in Transmission Electron Microscopy 14
2.6 SEM image of the dense AlNNWs at 1100 °C (8 μm scale bar); b) The TEM image shows AlN nanowire with 45 - 65 nm diameter. 14
2.7 Illustration diagram of Raman spectroscopy process. 15
2.8 Illustration on understanding the peaks in the raman spectrum. 16
2.9 Raman spectrum of the AlN nanowire films. 16
2.10 Image of the sonicator and probe station used in the device fabrication . . 17
2.11 The flexible PVC substrate utilized in the UV photodetector device fabrication. In the first step the substrate is cleaned in an ultrasonic bath. . . 18
2.12 In this step the freestanding AlNNWs films are transferred onto the PVC substrate. 18
2.13 The AlNNW film is masked and Au electrodes with a gap about 50 μm are sputter deposited on the channel. 19
2.14 Shows the flexible AlNNW film based UV photodetector. No lithography was used to pattern the electrodes. 19
2.15 Schematic diagram of the flexible AlNNW film based UV photodetector, and the photocurrent measurement set-up. Inset figure the actual image of the device. 20

3.1 The measurement setup for the AlNNW UV photodetector. 22
3.2 I-V characteristic of the fabricated flexible AlNNW device in dark condition. 23
3.3 IV curves of the AlNNW UV device under 254 nm UV (1.35 mW/cm^2 intensity) and in the dark conditions. 24
3.4 The photocurrent responses of the AlNNW photdetector at low bias voltages (1 V, 2 V and 5 V) under 254 nm UV light for 3 cycles. The photocurrent transients at 1 V bias shows very good sensitivity. Note: In Figure 3.4 d) the vertical axis scale (current) has been broken for better comparison of the photocurrent responses 26

3.5 Photocurrent-time response of the AlNNW UV photodetector under 254 nm UV light at higher bias voltages a) 10 V b) 12 V. 27
3.6 The photocurrent transients of the AlNNW photodetector at higher bias voltages of 12 V, 15 V, and 20 V under 254 nm UV light for 3 cycles. Note: The vertical axis scale (current) has been broken for better comparison of the photocurrent responses. 28
3.7 Photocurrent-time response of the AlNNW UV photodetector measured at 15 V bias under 254 nm UV light (6 W) for three 20-sec exposures. . . 29
3.8 Enlarged portions of the photocurrent transients at 15 V bias between 114 s and 146 s. The device exhibits quick rise and decay times (R_t and D_t) of 0.27 s and 0.41 s, respectively. 29

Abbreviations

Al_2O_3	Aluminum Oxide
AlN	Aluminum Nitride
AlNNW	Aluminum Nitride Nanowire
A	Area
BSE	Back scattered electrons
CVD	Chemical Vapor Deposition
EUV	Extreme Ultraviolet
FET	Field Effect Transistor
FUV	Far Ultraviolet
Ga_2O_3	Gallium Oxide
GaN	Gallium Nitride
LPCVD	Low Pressure Chemical Vapor Deposition
MEMs	Micro Electro Mechanical Systems
MSM	Metal/Semiconductor/Metal
MUV	Middle Ultraviolet
NEMs	Nano Electro Mechanical System
PMT	Photomultiplier tubes
p-n/p-i-n	P-type-N-type/ P-type-Intrinsic-N-type
SBR	Solar Blind Region
SE	Scattered electrons
SEM	Scanning Electron Microscopy
Si	Silicon
SiC	Silicon Carbide
SnO_2	Tin Oxide
TEM	Transmission Electron Microscopy

UV	Ultraviolet
UVPD	Ultraviolet Photodetector
V	Voltage
VLS	Vapor-Liquid-Solid
VUV	Vacuum Ultraviolet
WBG	Wide bandgap
XRD	X-Ray Diffraction
ZnO	Zinc Oxide
0D, 1D, 2D and 3D	Zero-, One-, Two- and Three-Dimension

Physical Constants

Speed of Light	c	$=$	$2.997\ 924\ 58 \times 10^{8}$ ms^{-S}
Electronic charge	q	$=$	1.602×10^{-19} C
Permittivity of vacuum	ϵ_0	$=$	8.854×10^{-14} F/cm

Symbols

Symbol	Name	Unit
E_g	Band gap energy	eV
$h\nu$	photon energy	eV
I_λ	Photocurrent	A
P_λ	Light intenisty	mW/cm^2
R_λ	Responsivity	mA/W
V_{ds}	Bias voltage	V
μ	Carrier mobility	$m^2/V.s$
η	Charge Carrier density	m^{-3}
σ	Conductivity	S/m

Chapter 1

Introduction

1.1 Summary

This thesis presents the fabrication and characterization of AlNNW film based UV photodetector via a cost friendly, practical and highly scalable scheme. The thesis is organized into the following four chapters:

- In chapter one, a broad classification of nanoscale UV photodetectors is discussed, followed by a brief introduction of low dimensional WBG semiconductor materials, specifically AlNNWs, as important blocks in the manufacture of electronic and optoelectronic devices.
- Chapter two details the experimental process in the fabrication of our AlNNW film UV photodetector, beginning with the synthesis of AlNNWs, their electrical & optical characterization and their integration as a nanoscale device. The equipment and the processes utilized are elaborated.
- The third chapter presents the electrical and photoconductive properties of the fabricated AlNNW device such as the I-V characteristics and the time-related photocurrent dynamics of the photodetector. More importantly, we compare the performance of our AlNNW UV photodetector with other reported low dimensional photonic devices.

- The final chapter concludes our findings and highlights the application opportunities presented by our UV photodetector as well as the future outlook of the next generation optical and photonic devices.

1.2 Low dimensional semiconductor materials

The advancement in fabrication methods has enabled nanostructure semiconductor materials to be realized in a more controlled and optimized way for large-scale technological applications through either top-down or bottom-up approaches. Bottom-up method provides flexibility in the synthesis of complex nanostructures tailor-made for specific applications. Among the nanostructures, one-dimensional semiconductor nanowires have been a subject of growing research interest due to their large surface-to-volume ratio, good crystal quality and superior properties in electronic and photonic applications. 1D nanostructures can be classified according to their shapes and sizes like: nanowires, nanotubes, naocables etc as summarized in table 1 below.

Nomenclature	**Diameter (nm)**	**Length (μm)**	**Cross-section**
Nanowires	1 - 100	1 - 100	Cylindrical
Nanotubes	1 - 100	1 - 100	Hollow
Nanorods	1 - 100	< 2	Cylindrical
Nanowhiskers	≥ 1000	10 - 1000	Cylindrical
Nanocables	1 - 100	1 - 100	Core-shell

Nanowires have been studied on the most among the above nomenclatures due to their simple structure which limits the presence of defects unlike typical crystalline semiconductors. Further, semiconductor nanowires growth can be realized on many different substrates via vapour deposition methods. Thus they present themselves as major building blocks for many integrated devices owing to their higher photosensitivity and photoconductive gain compared to bulk and thin film based devices. Photoconductivity, sensitivity to light radiation, is one of the most popular behaviour studied in nanowires and presents immense application opportunities in areas such as UV photodetection.

1.2.1 Ultraviolet light

UV light is the electromagnetic radiation (spectral band) between X-ray and Visible light and lies in wavelengths ranging from **10 nm** (124 eV) to **400 nm** (3.1 eV) [1]. As shown in table 2 below the main spectral regions can be classified as:

UV Type	Wavelength (nm)	Bandgap energy (EV)
UV-A	400 - 320	3.1 - 3.87
UV-B	320 - 280	3.87 - 4.43
UV-C	280 - 200	4.43 - 6.2
VUV	200 - 10	6.2 - 124

UV light with wavelength higher than 280 nm can penetrate to the earth's atmosphere therefore is referred to as Solar-blind while radiation with longer than 400 nm is called Visible-blind. Predominantly, UV light in the UVC and UVB regions which have higher energies and short wavelengths are absorbed by the ozone layer before reaching the earth's surface. However longer wavelength radiation above 300 nm (UVA) can easily penetrate to the earth's atmosphere and prolonged exposure can be hazardous and is known to cause health problems such as skin cancer [2]. Therefore it is extremely necessary to monitor the radiation's presence in the atmosphere. Furthermore, recently UV light has been utilized in various fields like medicine, agriculture and chemistry. High sensitivity, cost friendly and stable UV photodetectors are therefore required for the detection of UV radiation in the environment.

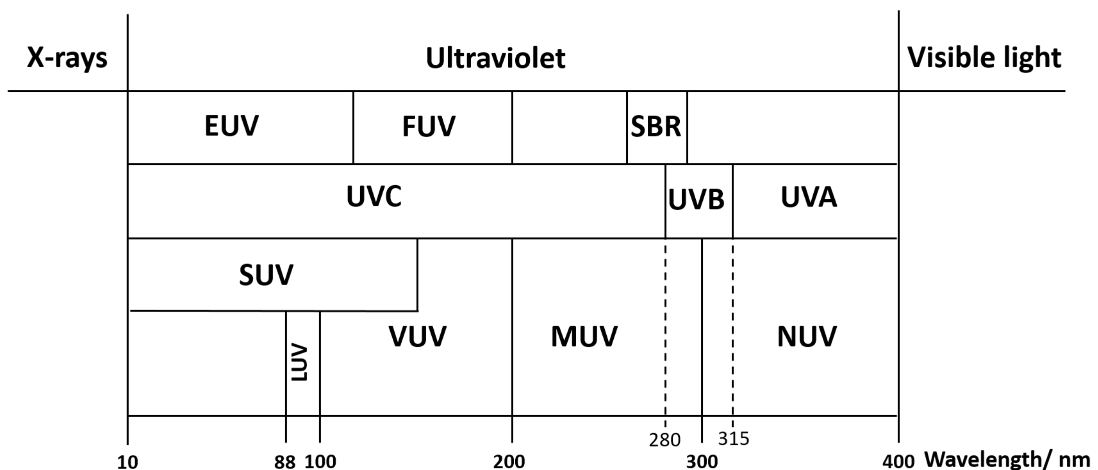

Figure 1.1: The commonly used spectral ranges of UV light.

All the spectral regions between the X-ray and Visible light wavelength are depicted in Figure 1.1 above.

1.2.2 UV detector types

UV detectors broadly fall under 2 categories: Vacuum UV detectors and Solid-state UV detectors. Vacuum UV detectors, which have been used in UV detection for a long time, are made up of Photomultiplier tubes (PMTs). However, they are bulky and consume a lot of power. Thus, the need for miniaturized and power efficient photosensors naturally led to the development of UV detectors based on semiconductors and they can be grouped by their active areas as either photoconductive or photovoltaic detectors. Semiconductor UV detectors offer unique advantages due to their small sizes such as increased sensitivity and low power consumption and have been utilized in vast application areas such as medicine, environmental monitoring, flame sensing, secure space communication, astronomical studies etc. [3–5]. The classification of these UV detectors is illustrated in Figure 1.2 below.

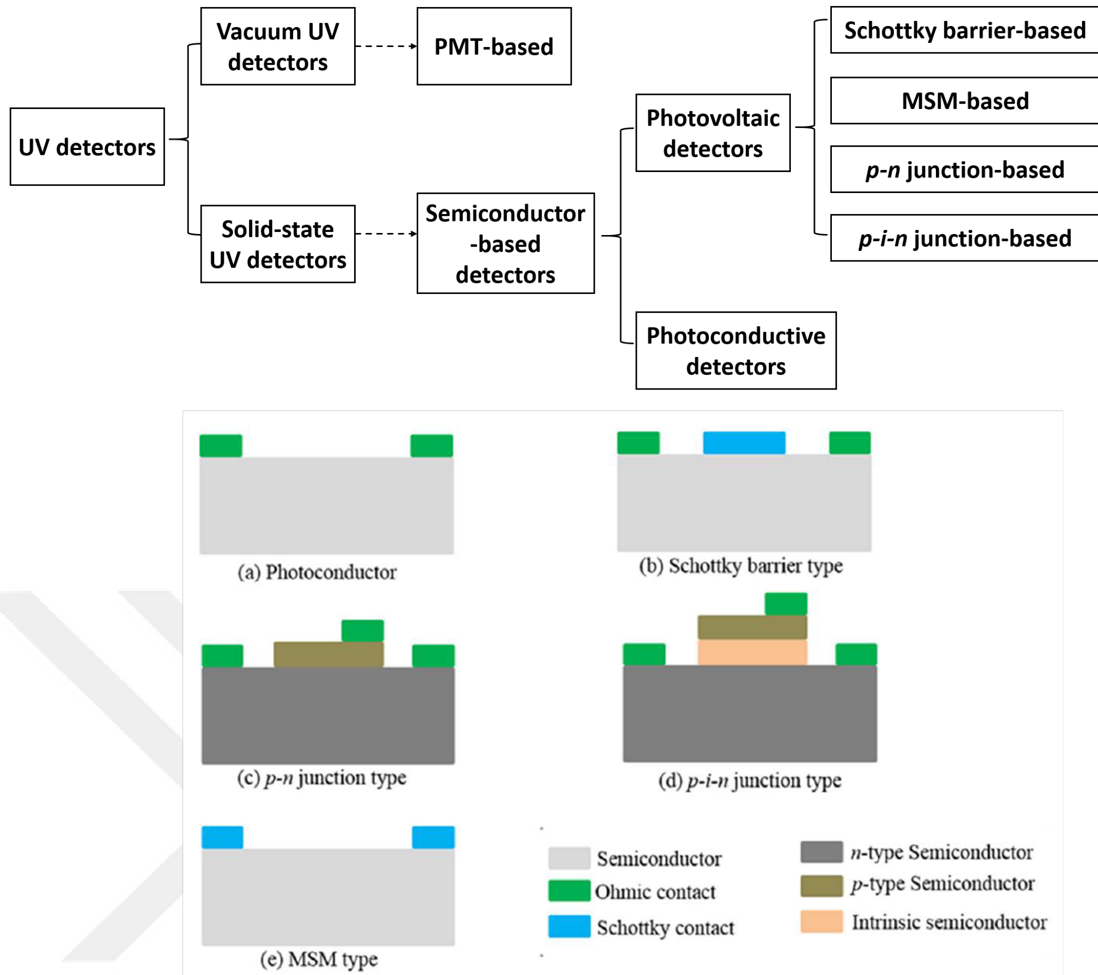

FIGURE 1.2: A classification of UV detector types as well as their schematic structure.

1.2.2.1 Photoconductive detectors

These detectors function based on the photoconductive principle. As shown in Figure1.2 a, they are made up of a semiconductor material and 2 ohmic contacts. The detector works by measuring the electrical conductivity fluctuations caused when an incident radiation with photon energy ($h\nu$) larger than the bandgap (E_g) is absorbed by the semiconducting material, resulting in electron-hole pair generation. Due to their simple structure, they present a less costly fabrication process and wide integration capability.

1.2.2.2 Photovoltaic detectors

1. **Schottky-barier detectors** - The schottky photodetector is formed by a metal and a semiconductor in contact, with a large barrier height. The metal-semiconductor junction shows a rectifying property caused by the work difference between the metal and semiconductor.

2. **MSM detectors** - It's structure comprises of 2 semiconductor schottky barriers joined together in a comb structure with the active region between the contacts for light absorption.

3. ***p-n* and *p-i-n* - junction detectors** A *p-n* junction or a photodiode is basically a *p-n* diode fabricated specifically to detect photons whereas the *p-i-n* junction includes an intrinsic layer separating the p and n doped regions as shown by their schematics in Figure 1.2 c and d.

1.3 Materials for UV photodetectors

UV photodetector's performance is fundamentally based on the intrinsic characteristics of the semiconductor material used to fabricate it. Wide bandgap (WBG, typically E_g between 3 eV - 6 eV) nanowire semiconductor materials have been desired in UV detector application due to the superior proprieties induced by their bandgap such as low permittivity, high breakdown electric field, high temperature operation, excellent oxidation and chemical inertness [6]. Furthermore their large surface area to volume ratio and miniature sizes enable them to yield a higher sensitivity to UV light. Compared to traditional semiconductor based detectors like silicon, WBG UV detectors offer larger bandgap selectivity and improved insensitivity to visible and infrared radiations. Thus, over the last decade, WBG have emerged as suitable candidates in manufacture of photosensitive devices such as UV photodetectors, phototransistors, photodiodes, photovoltaics, optical switches, transceivers and etc. In recent years, 1D WBG semiconductor nanomaterials such as ZnO, ZnS, SnO_2, SiC, Ga_2O_3, GaN [7–13] have been used to fabricate nanoscale UV photodetectors.

1.3.1 Aluminum Nitride (AlN)

Among these WBG semiconductor materials, AlN nanostructure, an important III-V WBG semiconductor, has been the subject of many studies because of its large direct bandgap (6.28 eV), low electron affinity, high thermal conductivity ($K \approx 320Wm^{-1}k^{-1}$), high melting point (above 2300°C), and chemical stability [14, 15]. Despite its intrinsic superior properties, challenges in synthesis of defect free and uniform morphology AlN nanostructures persist, thus so far few electrical and conductivity studies have been reported [16, 17]. Still they present a huge potential in the manufacture of next generation UV photodetectors [16, 18].

However, in order to manufacture these reported nanoscale UV photodetectors, conventional processes like lithography are used which can be complex, expensive and substrate limited. Driven by the growing demand for lightweight, portable and low-cost fabrication for electronics, flexible substrates are investigated for nanoscale device manufacturing. Hence, practical and inexpensive methods such as printing, spray coating, painting etc. have recently been demonstrated in fabricating flexible nanodevices [19–21].

Furthermore, in most cases for the devices to achieve good photocurrent high operating voltage is required, which may present a challenge for integration with low power consuming applications. For instance, Liu et al. reported an AlNNW based UV photoconductor operating at a voltage of 40 V [17]. Liang Li et al′s solar-blind Ga_2O_3 nanobelt UV photodetector records good response times under 30 V applied bias [22].

In this work, we present a low operating voltage flexible AlNNWs film UV photodetector fabricated via inexpensive and practical processes requiring no lithography. The device, which was prepared on a cheap polyvinyl chloride (PVC) substrate, exhibits excellent photoresponse properties and high sensitivity even at low bias voltage of 1 V, opening up new opportunities for integration with flexible photosensing applications. Furthermore, the time-dependent response behavior of the photodetector is examined at various bias voltages ranging from 1 V to 20 V. This study demonstrates the great potential of the AlNNWs in low-power consumption UV photosensing applications.

Chapter 2

Experimental details

2.1 AlNNW Growth

The AlNNWs were grown in resistively heated Low Pressure CVD (LPCVD) reactor. High purity Aluminum (99.97% purity and about 60 mg) in an alumina boat is loaded into the reactor chamber. During the catalyst free growth, Al powder which is used as a source material is directly put in the boat with no substrate and the growth occurs directly on the Al source. After that, high purity hydrogen is then purged through the reaction chamber in three cycles to clear any present contaminant gases. Following purging, the reactor is heated to growth temperature of 1100 °C with hydrogen gas as a carrier. Once the growth temperature is reached, high purity ammonia and hydrogen carrier gases with a flow rate of 300 sccm are introduced into the reactor chamber for 120 minutes. Once the growth process finishes, ammonia is turned off and with only hydrogen flowing the system is cooled down to 250 °C before the furnace is unloaded and let to further cool to room temperature. The catalyst-free growth process can be summarized as follows: Early in the heating process the Al powders melts to form a film as the melting point of Aluminum is reached at 650 °C. When the process nears the growth temperature (1100 °C), the Al film slowly disintegrates to form clusters due to hydrogen gas's reducing effect [23, 24]. As NH_3 flows through the chamber, the reaction below occurs:

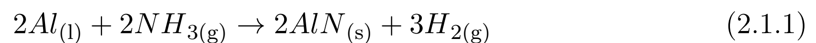

$$2Al_{(\mathrm{l})} + 2NH_{3(\mathrm{g})} \rightarrow 2AlN_{(\mathrm{s})} + 3H_{2(\mathrm{g})} \tag{2.1.1}$$

Figure 2.1: MOCVD equipment used for the growth of the nanowires. The lower image depicts the quartz tube inside where the reaction occurs.

2.2 NW Characterization

To image and characterize the as-grown nanowires we employed the following nanocharacterization devices:

1. Scanning Electron Microscope (SEM, Phenom XL)
2. Transmission Electron Microscope (TEM, JEOL JEM 1011)
3. Raman Spectrometer (Reinshaw inVia Raman microscope with 532 nm laser excitation and Leica DMLM microscope)

2.2.1 Scanning Electron Microscope (SEM)

The Scanning Electron Microscope is designed to study the surfaces of solid specimens using electron beams in focus inducing generation of signals from the electron-surface interaction that reveal morphology, chemical composition, structure and orientation of the sample. It consists of an electron generating gun, a column where the electron beam passes, a series of lenses to focus the electron beam, a chamber that houses the sample and a number of pumps for low vacuum operation. The accelerated electrons generate an array of signals caused by the electron and surface interaction which include the secondary electrons (SE), Back-scattered electrons (BSE) and diffracted back-scattered electrons. SEs, emitted from the specimen's surface, are the most valuable as they reveal the morphology and topography of the sample, while the BSEs are those that are scattered backward from the specimen when the incident electrons hit the surface. They contain contrast information of the sample. Figure 2.1 depicts the SEM equipment used to image our nanowires (Phenom XL) and the layout illustrating the working mechanism [25].

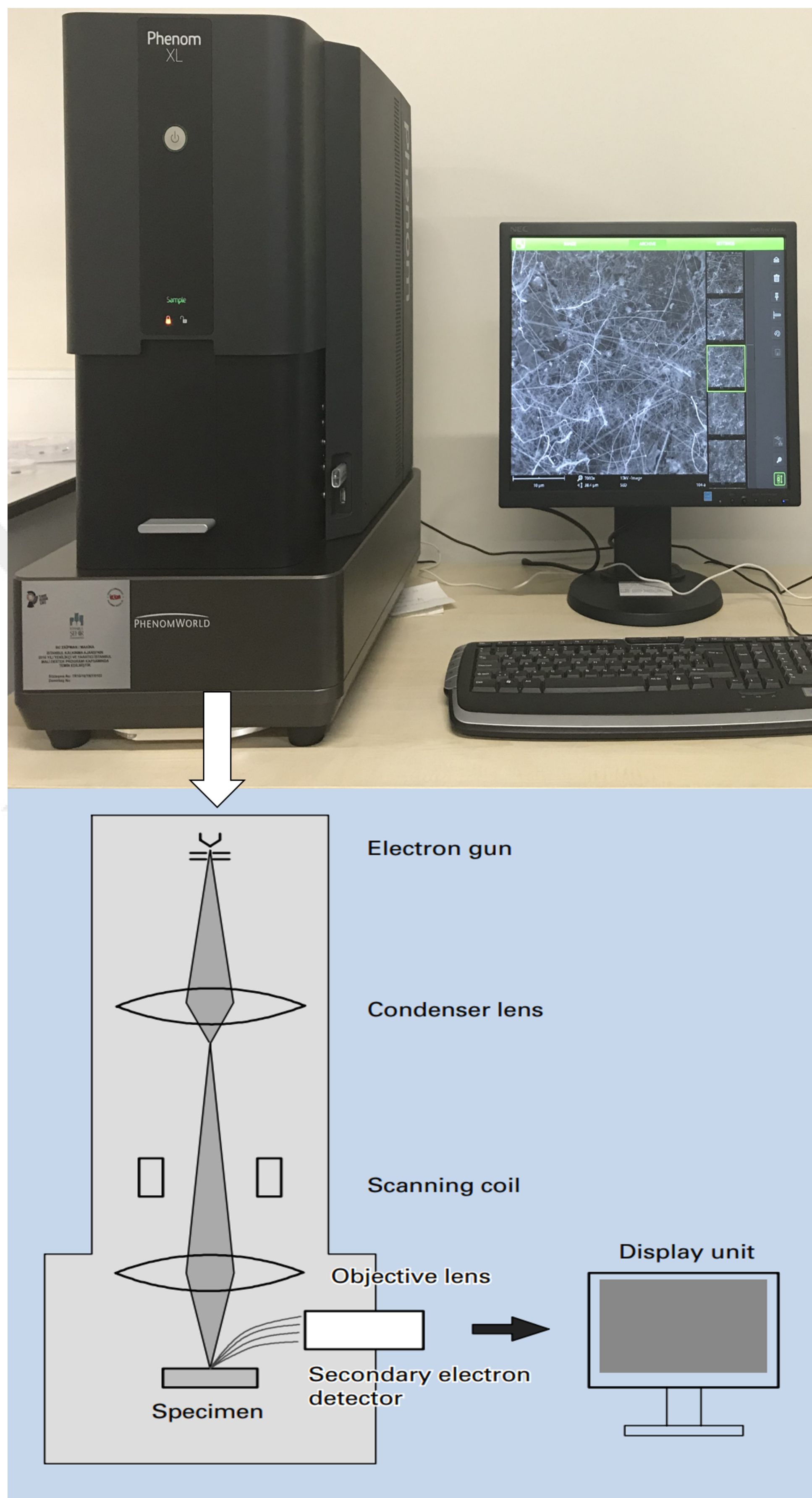

FIGURE 2.2: SEM (Phenom XL) used to image the nanowires. Its mode of operation is illustrated in the bottom figure.

Below are the high and low magnification SEM images of the dense AlNNW films grown catalyst free at 1100^{0}C. The AlN nanowires growth took place directly on the source mixture of Al-Al_2O_3, which was placed to an alumina boat without any substrate. These AlN nanostructure films were then placed on an SEM sample holder using conductive carbon tape. The AlNNWs have lengths and diameters ranging from 5 - 10 μm and 45 - 65 nm, respectively.

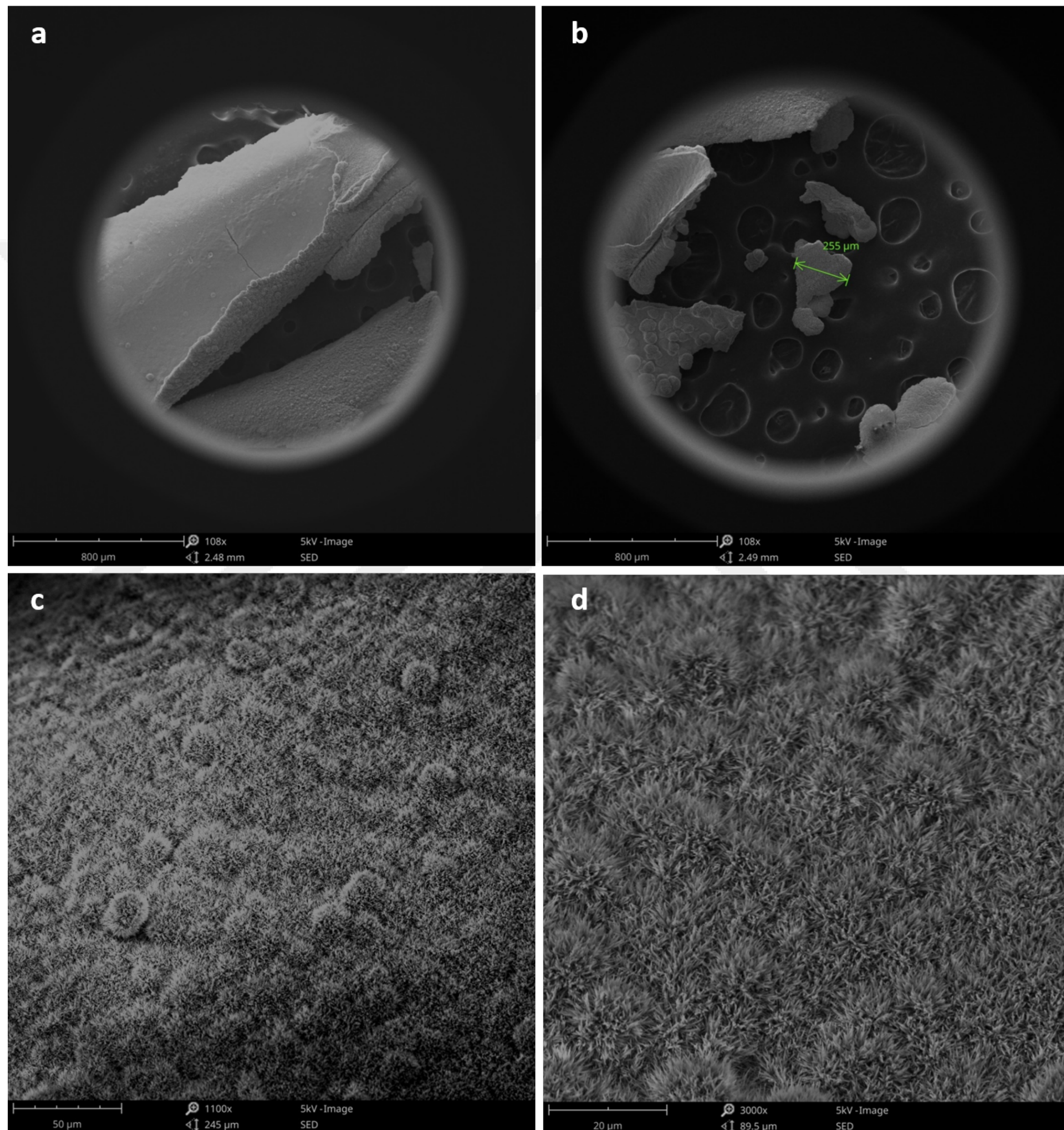

FIGURE 2.3: SEM images of the dense AlNNW films grown catalyst-free at 1100 °C at low magnification. a) 100x b) 300x c) 1100x d) 3000x

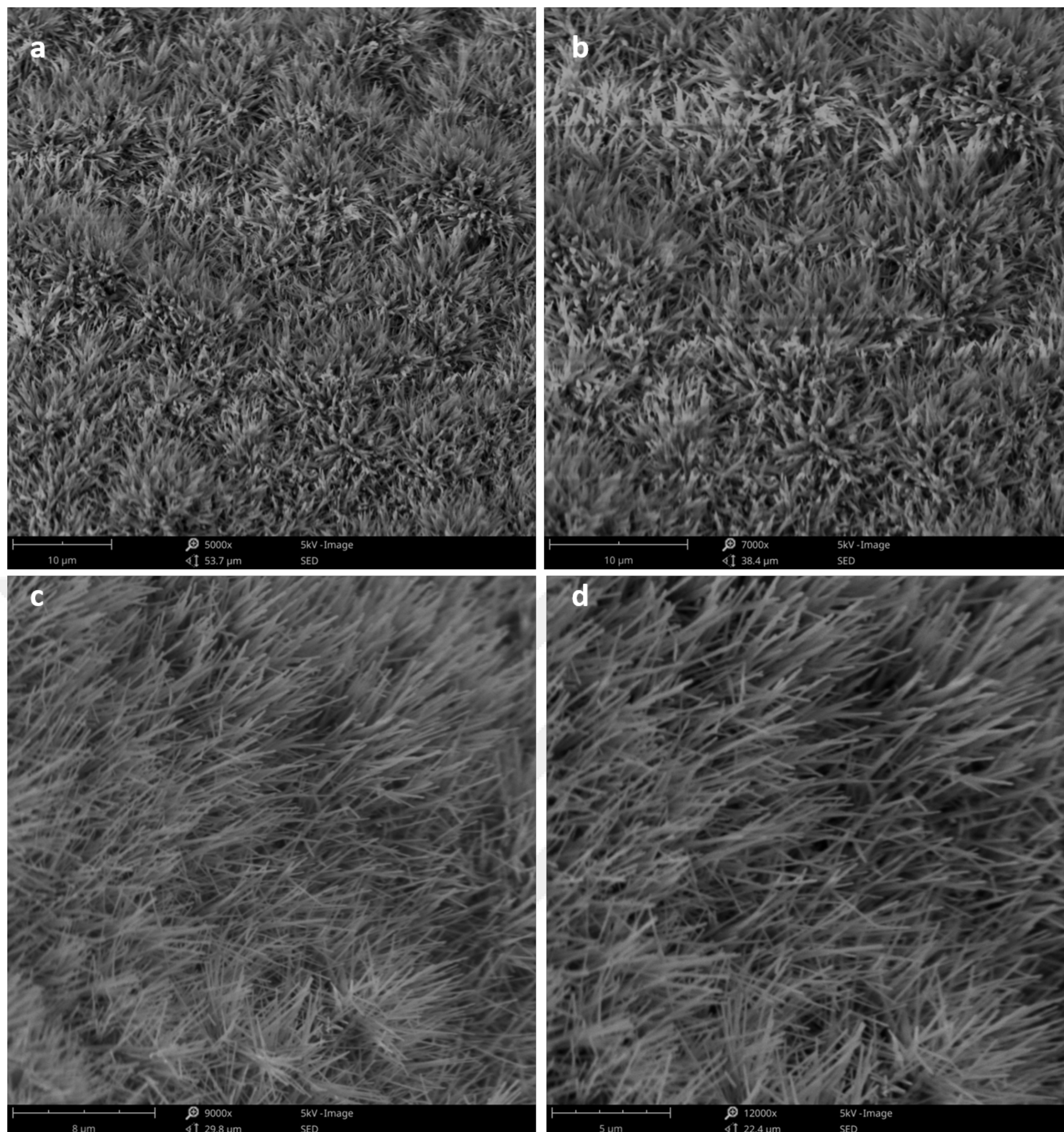

FIGURE 2.4: SEM images of the AlNNW films at higher magnification. a) 5000x b) 7000x c) 9000x d) 12000x

2.2.2 Transmission Electron Microscope (TEM)

Transmission Electron Microscope follows a similar principles of operation as a light microscope, but uses electrons instead of light. TEM images samples using high energy electrons (upto 300 kV accelerating voltage) generated at high speed within a vacuum and detecting the transmitted electrons through the sample. While passing through the sample electrons get deflected or stopped at some regions of the sample more than others. The dark spots indicate the parts where the electrons did not pass through. This electron-atom interaction can be used to observe the crystal structure, composition and

defects in semiconductor samples. It can capture high magnification at 1,000,000x and a resolution of below 1 nm. Figure 2.5 illustrates the imaging principle of the TEM[25].

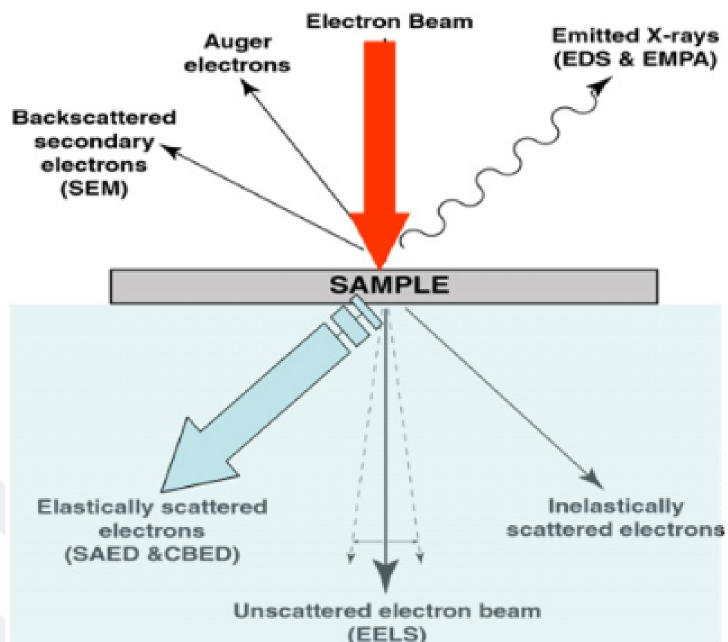

FIGURE 2.5: Electron-atom interaction in Transmission Electron Microscopy

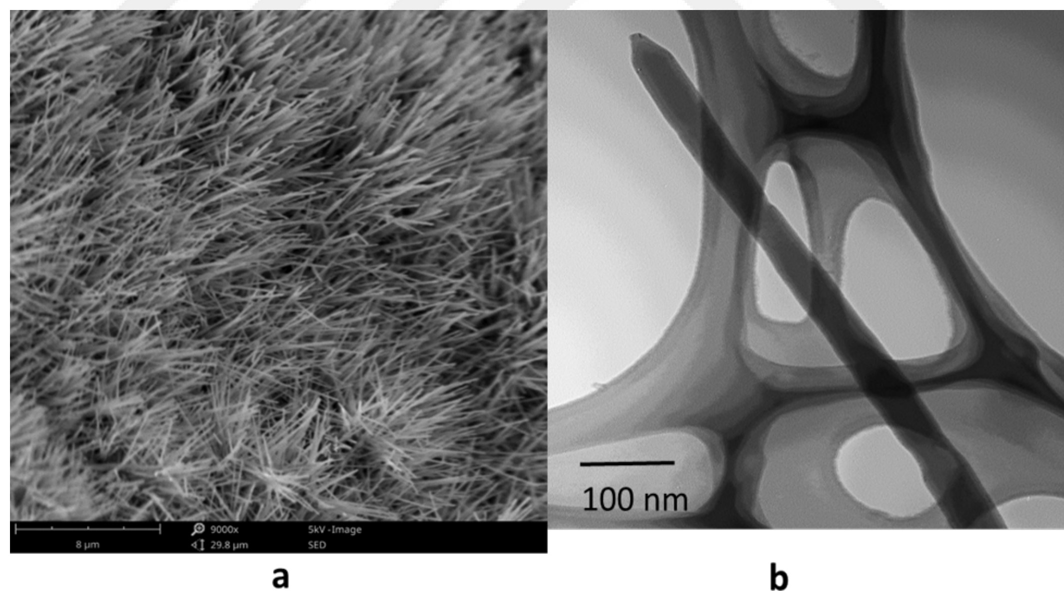

FIGURE 2.6: SEM image of the dense AlNNWs at 1100 °C (8 μm scale bar); b) The TEM image shows AlN nanowire with 45 - 65 nm diameter.

Figure 2.6 b shows TEM image of an AlN nanowire with lengths of 10 of microns and diameters of about 45-65 nm. The nanowire slightly tapers towards the tip, with its diameter shrinking as seen in the TEM image.

2.2.3 Raman Spectroscometer

It is a non-destructive contact-free spectroscopic technique used to provide information on the crystal structure and molecular vibration of a sample. This method uses a monochromatic light source to illuminate a sample, generating scattered light with unchanged energy (Rayleigh scattered) and a small fraction which has gained or lost energy (Raman scattered). Where the scattered light has lost energy it is referred to as stokes and in the case the scattered light has gained energy is referred to as anti-stokes. The Raman spectra basically gives the molecular fingerprint of the sample. Figure2.8 illustrates the basic raman spectroscopy principles [26].

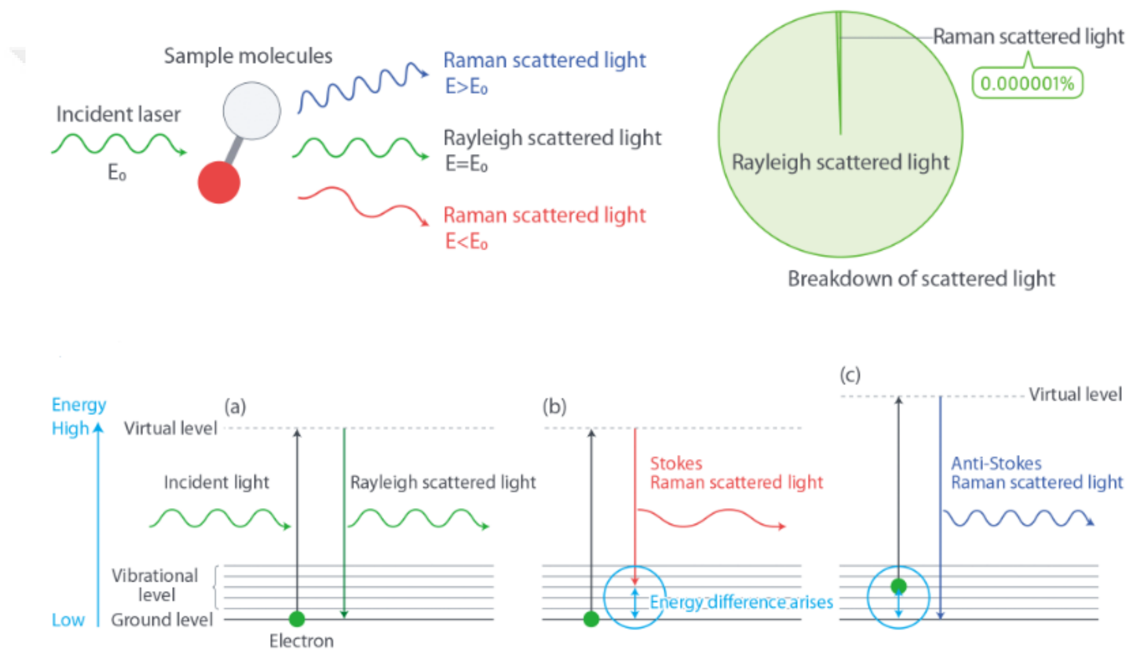

FIGURE 2.7: Illustration diagram of Raman spectroscopy process.

Figure 2.9 shows a Raman spectrum of the AlN nanowires. Raman spectroscopy is a very practical analysis tool used to analyze the optical quality and crystalline structure of nanomaterials. The Raman spectrum peaks are yielded at 611 cm^{-1}, 656 cm^{-1}, 668.3 cm^{-1}, and 907.4 cm^{-1} which corresponds to (A1; TO), (E2; high), (E1; TO) and (A1; LO) respectively. The peaks concur well with the high-quality, single-crystalline bulk AlN. The E2 (high) mode is used to analyze the stress state of AlN crystals because of its high sensitivity to stress [27]. Thus, the sharp and strong E2 (high) peak demonstrates the excellent crystal quality of the as-grown AlNNWs.

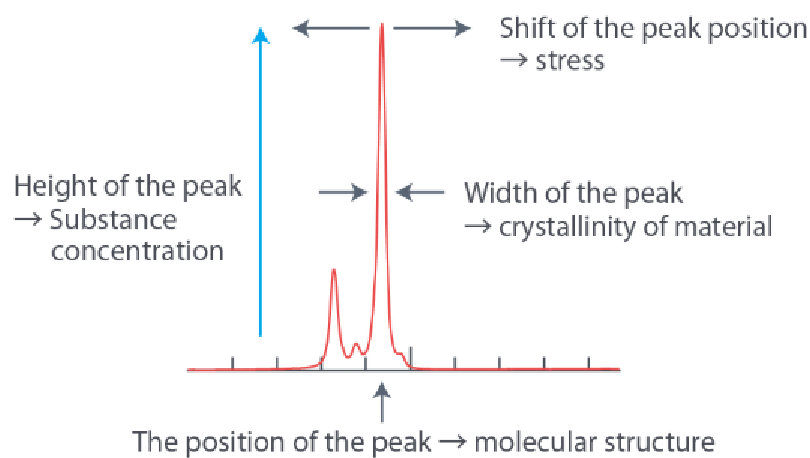

FIGURE 2.8: Illustration on understanding the peaks in the raman spectrum.

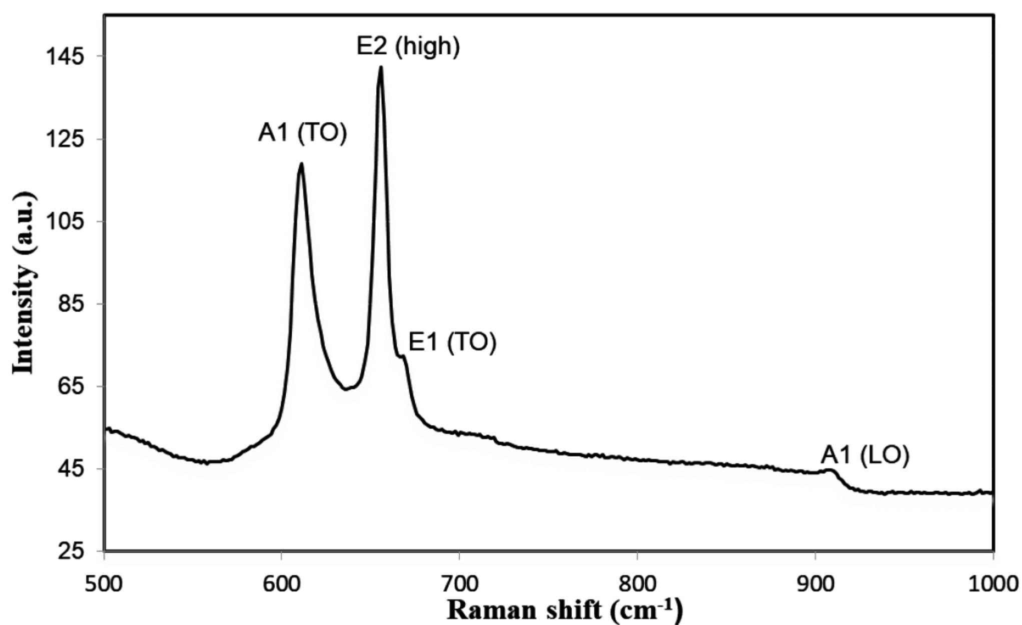

FIGURE 2.9: Raman spectrum of the AlN nanowire films.

2.3 Device Fabrication

To study the electrical and photoconductive properties of the dense catalyst-free grown AlNNW films, a flexible UV photodetector device was fabricated in four main steps:

- **Step I** - Substrate preparation and cleaning via IPA sonication
- **Step II** - The deposition of the AlNNWs on the substrate.
- **Step III** - Masking and the deposition of the Au electrodes on the nanowire network channel.
- **Step IV** - Mask removal and drying of the as-prepared AlNNW based UV photodetector.

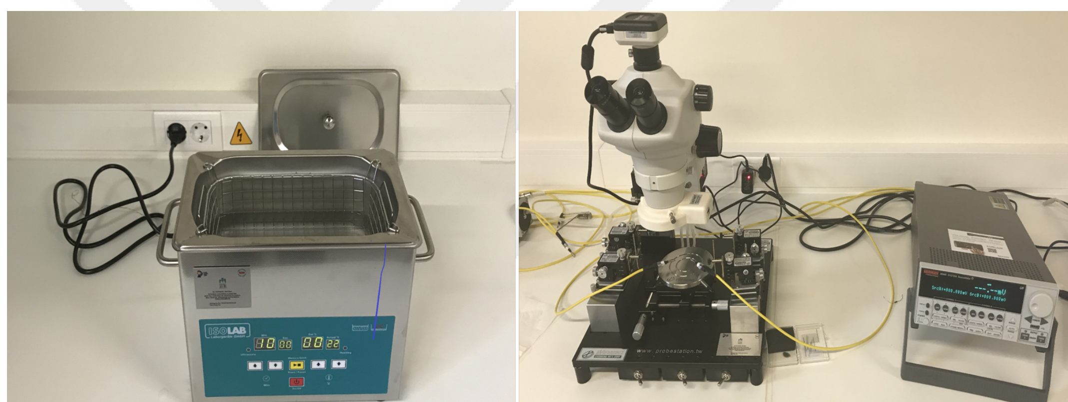

FIGURE 2.10: Image of the sonicator and probe station used in the device fabrication

First, a flexible low cost PVC substrate was prepared (10 mm by 10 mm with a thickness of 1 mm). The substrate was sonicated in IPA for 5 minutes then rinsed in deionized water to clean the surface. This also enhanced the surface improving the polymer-metal adhesion. Next, AlNNW networks were carefully placed onto the PVC substrate. The surface is then masked and Au electrodes with 50 μm gap are sputter deposited. The Au deposition lasted for 20 seconds at 20 mA. No lithographic process was used in the patterning of the electrodes, hence the fabrication scheme is very practical and readily scalable, and offers great advantages of integration capability with many substrates particularly in the growing flexible electronics market. The device fabrication steps is illustrated in the schematic Figures 2.11 - 2.14 below.

2.3.1 Substrate preparation and cleaning.

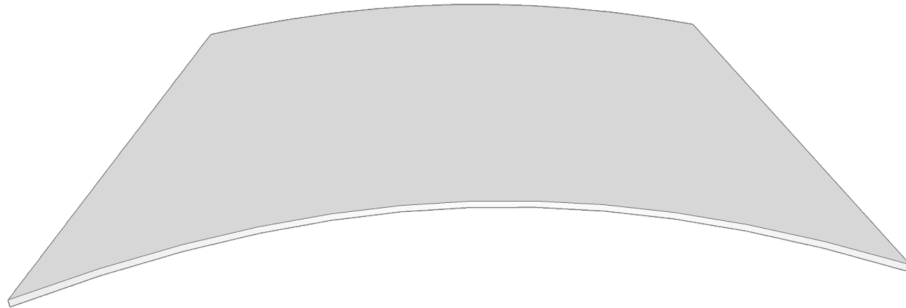

FIGURE 2.11: The flexible PVC substrate utilized in the UV photodetector device fabrication. In the first step the substrate is cleaned in an ultrasonic bath.

2.3.2 The deposition of the AlNNWs on the substrate.

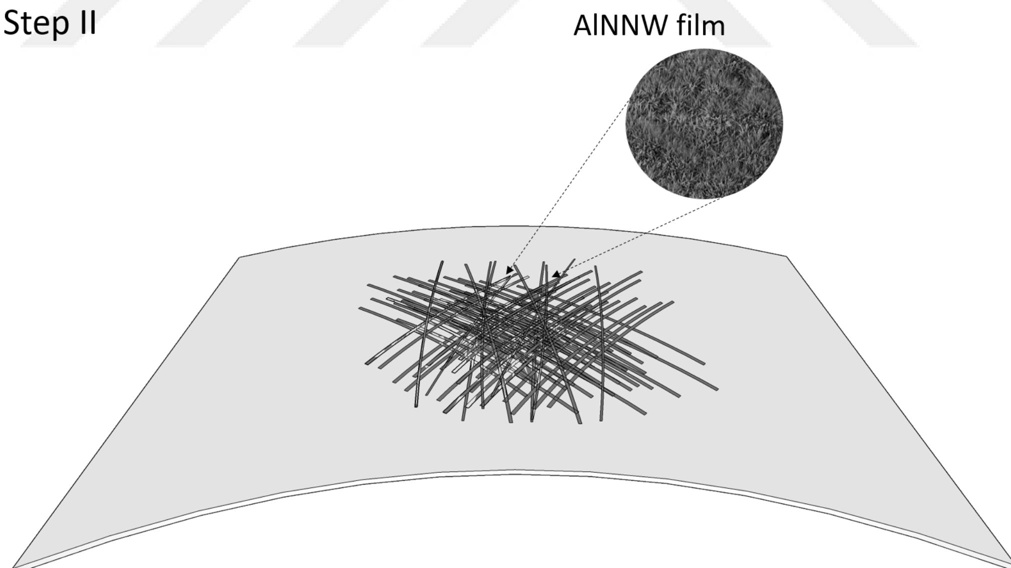

FIGURE 2.12: In this step the freestanding AlNNWs films are transferred onto the PVC substrate.

2.3.3 Masking and the deposition of the Au electrodes on the nanowire network channel.

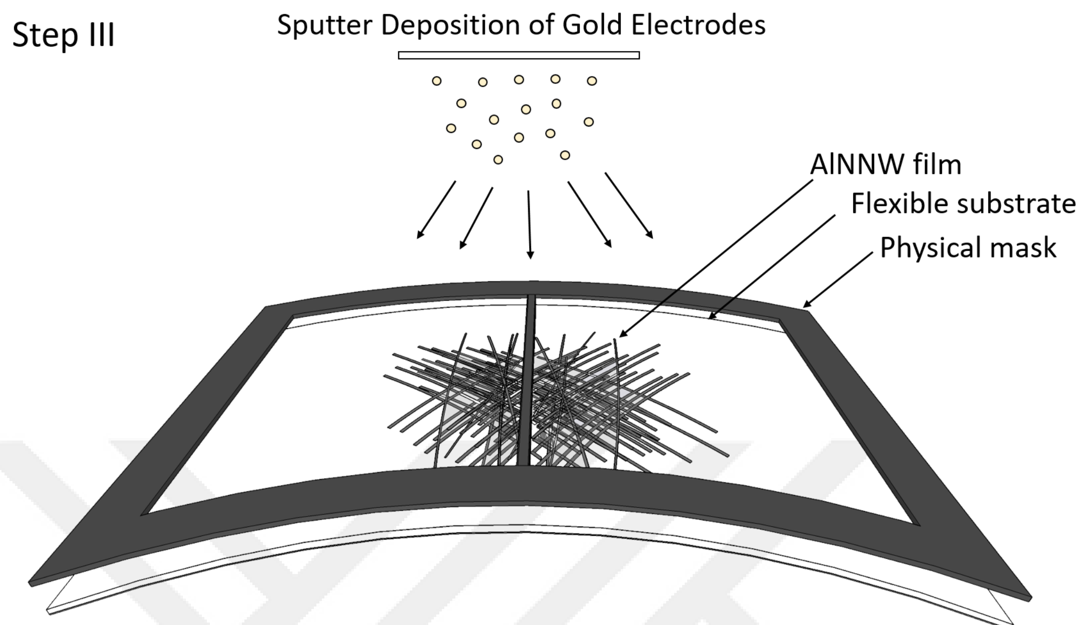

FIGURE 2.13: The AlNNW film is masked and Au electrodes with a gap about 50 μm are sputter deposited on the channel.

2.3.4 The flexible AlNNW based UV photodetector.

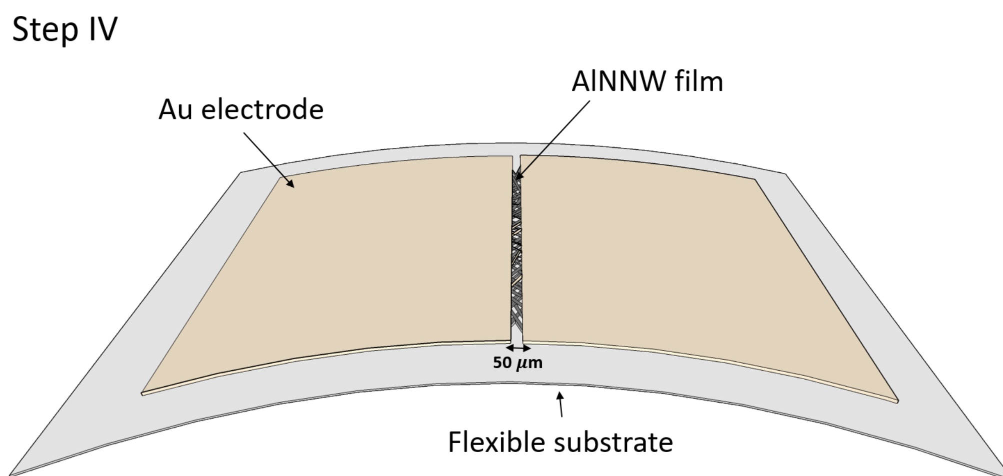

FIGURE 2.14: Shows the flexible AlNNW film based UV photodetector. No lithography was used to pattern the electrodes.

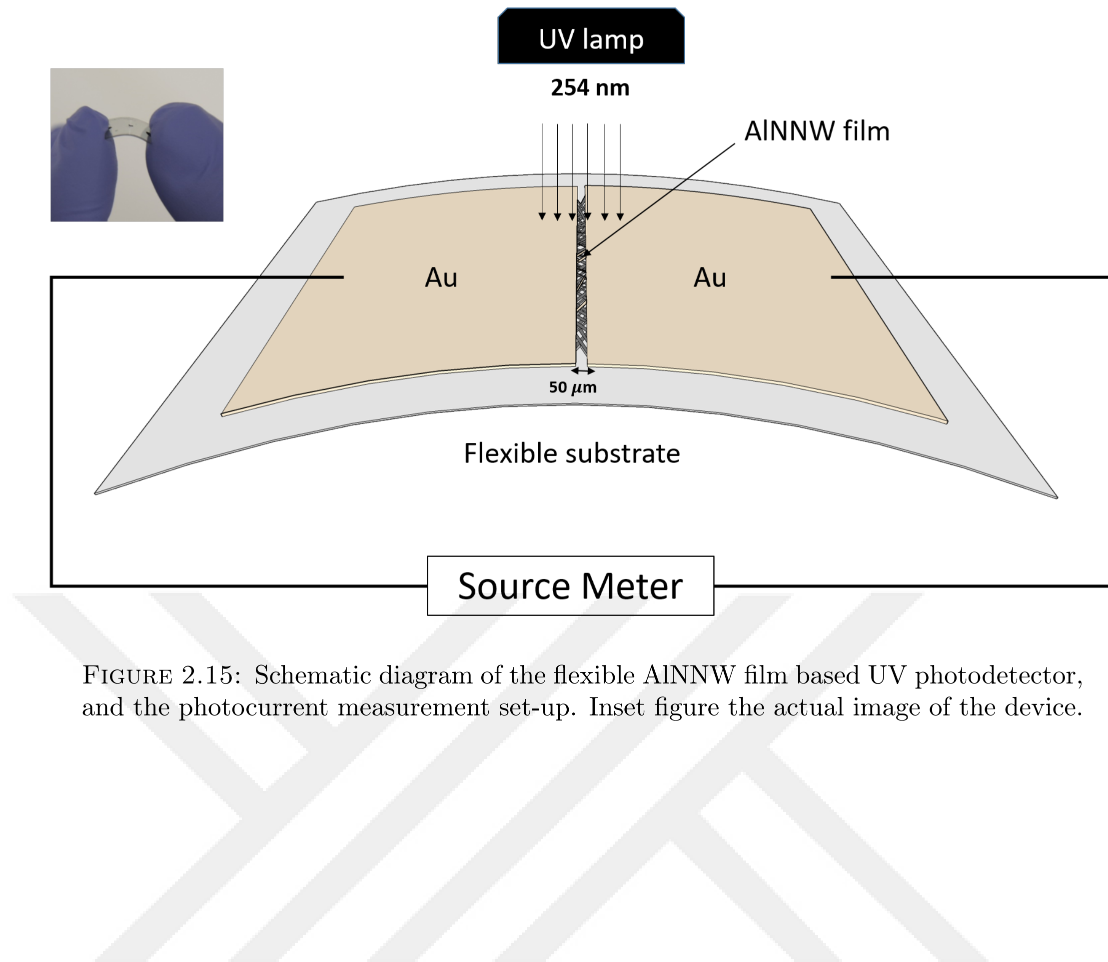

FIGURE 2.15: Schematic diagram of the flexible AlNNW film based UV photodetector, and the photocurrent measurement set-up. Inset figure the actual image of the device.

Chapter 3

Photoconductive properties of flexible AlNNW UV photodetector

3.1 Introduction

Photoconductivity in semiconductor nanowire materials has been studied upon a lot, especially in the application of nanowire photodetectors. It is the phenomenon where the electrical conductivity of a material increases due to the absorption of incident radiation. These characteristics in semiconductor nanomaterials are crucial in designing efficient optoelectronic devices which can open up new opportunities in fast switching and highly sensitive components. The intrinsic conductivity of a semiconductor material in the absence of illumination is described by the equation 3.1.1 below [28]:

$$\sigma = e\eta\mu \tag{3.1.1}$$

Where σ, e, η and μ stand for the conductivity, electronic charge, the charge carrier density and the carrier mobility. Upon UV light illumination the conductivity change is mainly caused by the increase or decrease in carrier concentration or in carrier mobility.

$$\Delta\sigma = \sigma_{\text{light}} - \sigma_{\text{dark}} = e\mu\Delta n + en\Delta\mu \tag{3.1.2}$$

The magnitude of increase or decrease in conductivity caused by the incident irradiation depends on the number of the carriers photogenerated.

3.2 Current - Voltage (I - V) characteristic

The I-V characteristics reveal the relationship between the current passing through the device and the supplied bias voltage. It defines the basic behavior of the device under electric circuit operation. The I-V and photocurrent of the device were measured by Keithley 2634B as shown by the setup in Figure3.1. A 6W 254 nm (1.35 mW/cm^2 intensity) and 365 nm (1.2 mW/cm^2 intensity) light sources were used for time response measurements.

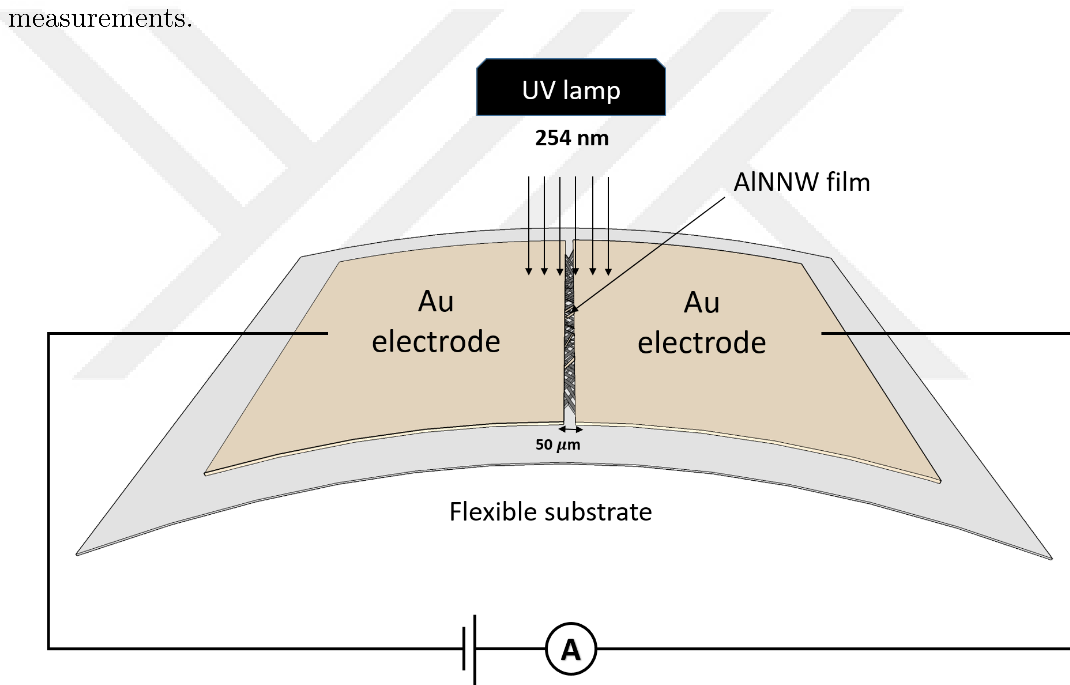

FIGURE 3.1: The measurement setup for the AlNNW UV photodetector.

Figure 3.2 shows the I-V curve of the AlNNW device under no UV illumination i.e. in the dark condition condition. The curve was linear indicating the ohmic behaviour of the contact between the AlN nanowires and the gold electrodes. Furthermore the current - voltage curve demonstrates the presence of good contact between the nanowires and the electrodes despite the lithography-free practical and cost efficient fabrication scheme.

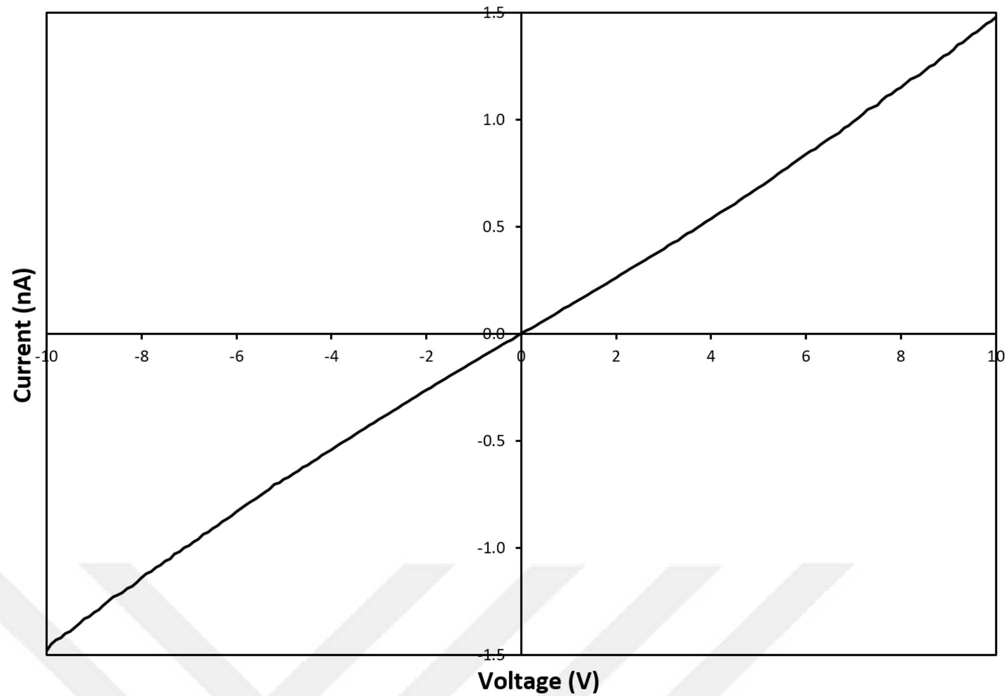

FIGURE 3.2: I-V characteristic of the fabricated flexible AlNNW device in dark condition.

Subsequently, the device was illuminated under 254 nm and 365 nm UV light to further investigate its current-voltage behaviour. The device shows a significant increase in photocurrent after UV exposure as seen in the curves in Figure 3.3. The photogenerated carriers cause an increase the conductivity as the nanowire is irradiated by photons with higher energy than the bandgap [29, 30]. Furthermore, we observe that the photogenerated current increases with the decrease in the UV light wavelength. This can be attributed to the higher photon energy of the electrons in 254 nm wavelength compared to 365 nm light that leads to the increase in the number of photogenerated carriers as shown by equation 3.1.2.

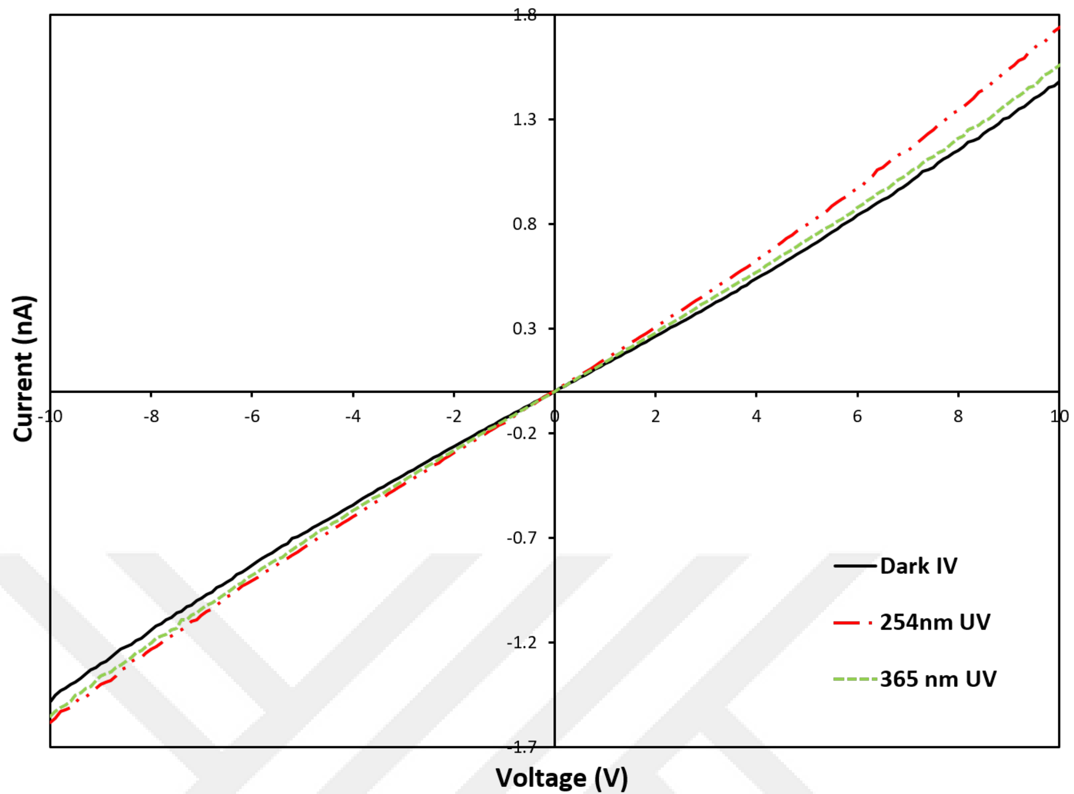

Figure 3.3: IV curves of the AlNNW UV device under 254 nm UV (1.35 mW/cm^2 intensity) and in the dark conditions.

Furthermore, under 254 nm irradiation the photocurrent increases by about 5% at lower bias voltages (1V - 5V) and around 3.5% at higher bias voltages (10V - 20V) as shown in Figure 3.3 below. The positive photocurrent response can be explained by the molecular sensitization phenomenon as reported in other nanostructures [31–33]. According to this mechanism, free electrons in the AlN nanowire surface capture oxygen molecules to form negative oxygen ions. As the free electrons move further away from the surface due to the negative oxygen ion adsorption, a low conductivity electron depletion layer is formed at the nanowire surface. Consequentially, the conductive path of the electrons in the AlN nanowire turn narrow resulting in an increase in the nanowire resistance. Upon UV illumination as photon energy ($h\nu$) exceeds the band gap energy (E_g), incident light is absorbed by the nanowire resulting in electron-hole pair generation [$h\nu \rightarrow e^- + h^+$]. The generated holes can move to the depletion layer at the surface thereby discharging the negative oxygen ions. Hence oxygen photo-desorption from the surface occurs as shown in the equation below:

$$h^+ + O_2^- \rightarrow O_2(g) \tag{3.2.1}$$

With the release of O_2 gas, an increase in the electron channel width leads to the decrease in resistance at the surface of the nanowire, hence the positive photocurrent response. Upon turning off the UV light, the photo-generated electron-hole pair rapidly vanish leading to the decrease in photocurrent.

3.3 Response times

Having achieved very good current-voltage results, the photocurrent time response characteristics of the device was examined by periodical exposure to UV light of 254 nm and 365 nm wavelength under different bias voltages.

3.3.1 Response times at low voltages

First, 254 nm UV light was irradiated on the device at bias voltages of 1 V, 2 V and 5 V as shown in Figure 3.4. The UV light was kept ON & OFF for 20 seconds in each cycle and repeated for 3 cycles. It is observed (as expected) that the photocurrent increase immediately after illumination is proportional to the applied bias voltage. Interestingly even at these low bias excitations of 1 V, 2 V and 5 V, our device exhibits quick rise ($<$ 1 s) and recovery ($<$ 2 s) times, as shown by the photocurrent transients in Figure 3.4. This good sensitivity can be attributed to the good optical quality of the AlN nanowires and the good contact quality between the Au electrodes and AlNNWs. However, it is worth noting that the response times obtained at these low voltages were not taken into consideration due to the limitation of our current measurement system. We expect the measurement induced errors can be removed if the data collection frequency could be auto-controlled by a quicker software script and the actual response times at low bias voltage will be faster than the measured values. Further, it is important to point out that as bias voltage increases, the photocurrent increases as well. In fact, the photocurrent at 5 V is approximately four times larger than the photocurrent at 1 V. The bias-voltage dependence of the photocurrent increase has been reported for other material systems, and this can be attributed to the increase in carrier drift velocity and reduction of the carriers transit time as shown by the equation below:

$$t = l^2/(\mu.V_{\mathrm{ds}}) \tag{3.3.1}$$

where l, μ and V_{ds} are the device length, the carrier mobility, and applied bias voltage, respectively [34, 35].

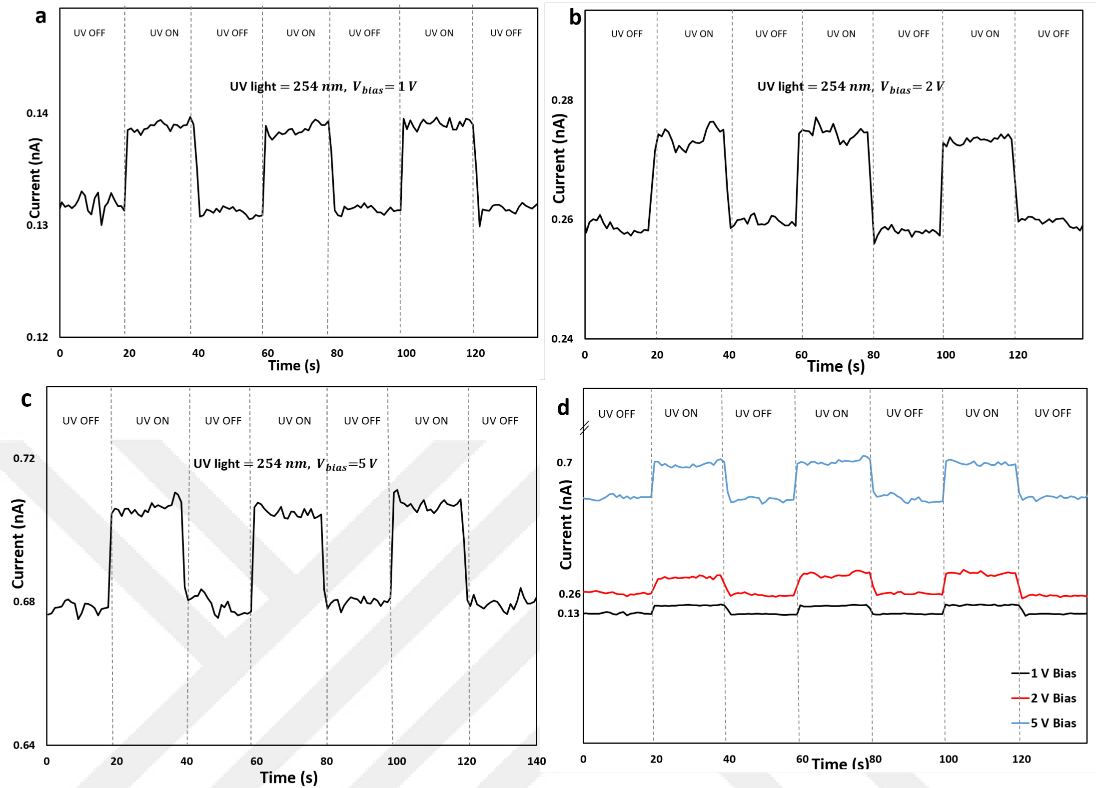

FIGURE 3.4: The photocurrent responses of the AlNNW photdetector at low bias voltages (1 V, 2 V and 5 V) under 254 nm UV light for 3 cycles. The photocurrent transients at 1 V bias shows very good sensitivity. Note: In Figure 3.4 d) the vertical axis scale (current) has been broken for better comparison of the photocurrent responses

3.3.2 Response times at high voltages

Next, the AlNNW photodetector was illuminated under 10 V, 12 V, 15 V and 20 V to monitor the effect of bias voltage on the photoresponse behavior of the AlNNW device in saturation. As demonstrated by Figure 3.6 the time-related photocurrent response is a function of bias voltage and an increase in photocurrent is clearly observed with applied voltage. A stable photocurrent increase of up to 0.1 nA is measured upon UV illumination. At maximum bias voltage of 20 V the photocurrent is approximately 17 times bigger than the lowest bias voltage at 1 V. Even though the current on/off ratio is small, the AlNNW device demonstrates excellent stability with increasing voltage. In fact, we can expect a higher photocurrent at larger bias voltages, but to maintain low power consumption our photodetectors must operate at low bias voltages.

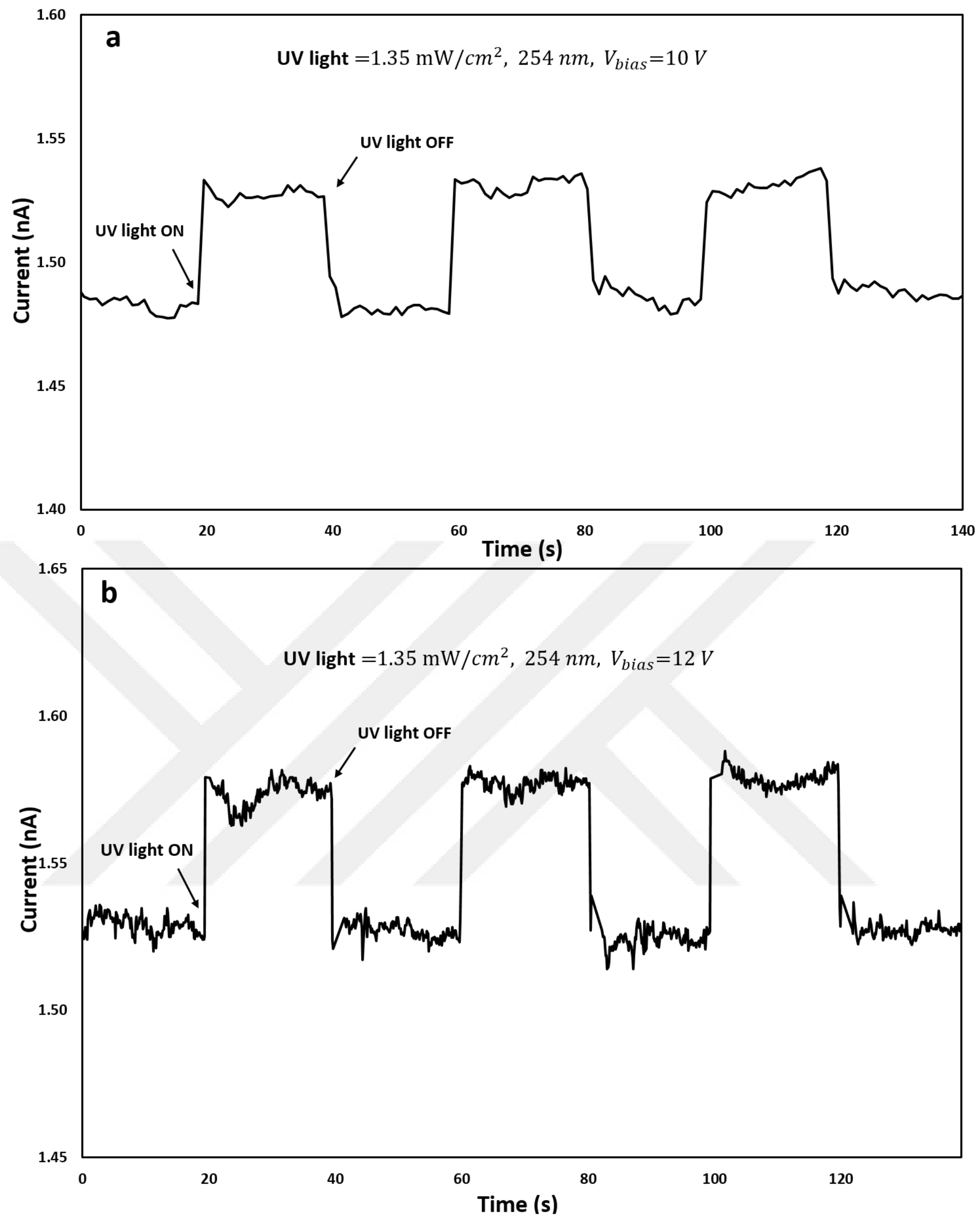

Figure 3.5: Photocurrent-time response of the AlNNW UV photodetector under 254 nm UV light at higher bias voltages a) 10 V b) 12 V.

Notably as well, during the repeated periodical UV exposures, the photocurrent quickly decayed to its dark current level, after the UV light was turned off showing no sign of persistent photoconductivity. This shows the great reversibility and stability of the AlNNW photodetector device. The absence of this persistent photocurrent can be explained by the complete depletion of the space charge layer [36] and the absence of intrinsic structural defects or point defects in the AlN nanowires leading to an enhanced electron-hole recombination process.

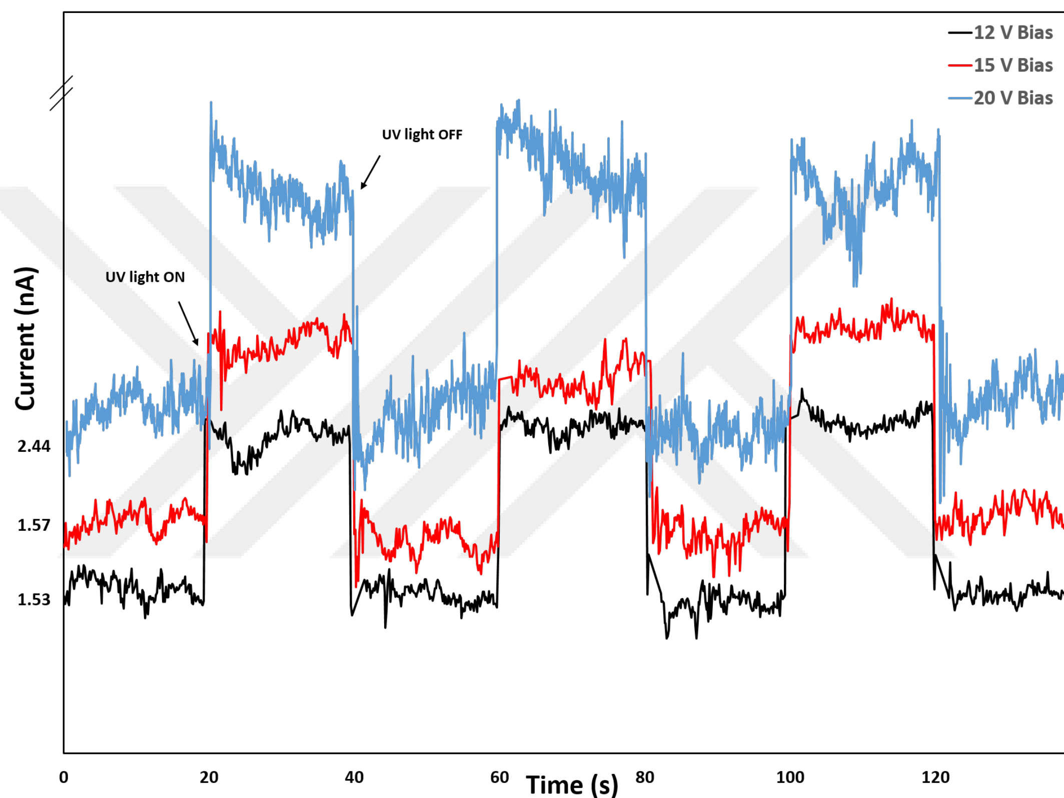

FIGURE 3.6: The photocurrent transients of the AlNNW photodetector at higher bias voltages of 12 V, 15 V, and 20 V under 254 nm UV light for 3 cycles. Note: The vertical axis scale (current) has been broken for better comparison of the photocurrent responses.

3.3.3 Rise time and decay time

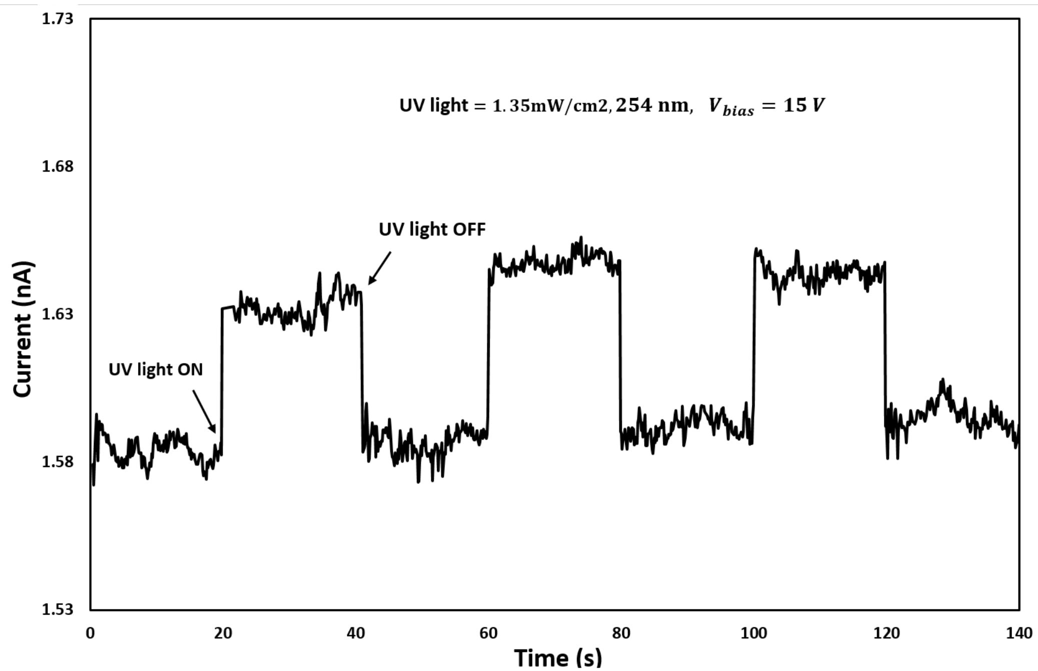

Figure 3.7: Photocurrent-time response of the AlNNW UV photodetector measured at 15 V bias under 254 nm UV light (6 W) for three 20-sec exposures.

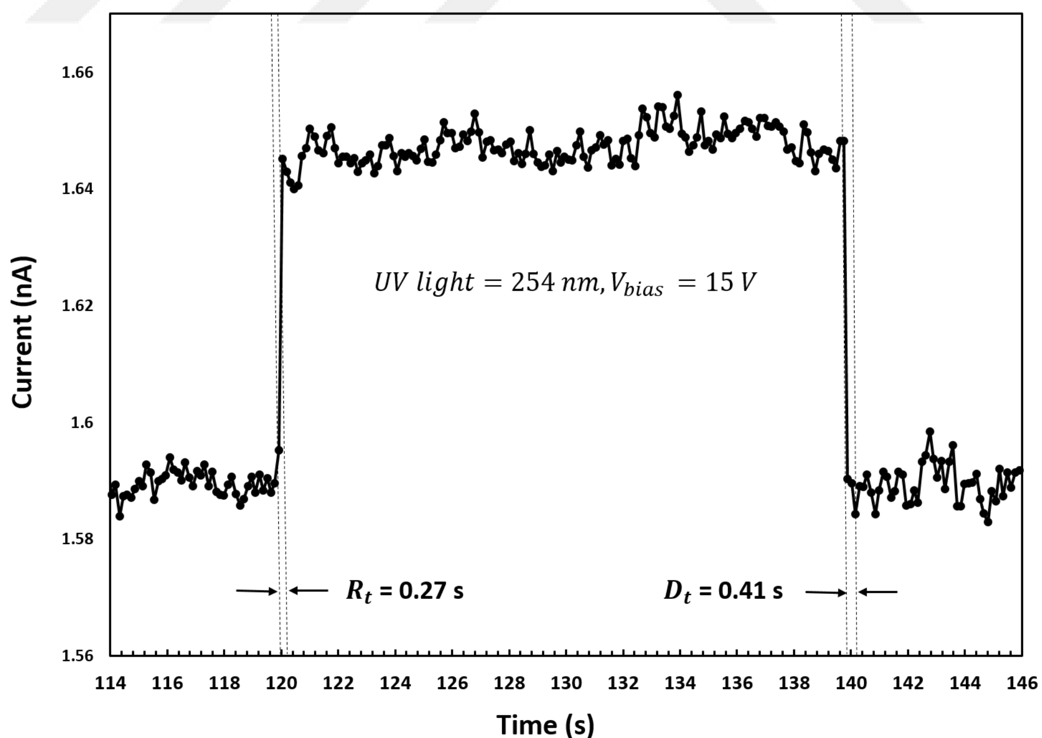

Figure 3.8: Enlarged portions of the photocurrent transients at 15 V bias between 114 s and 146 s. The device exhibits quick rise and decay times (R_t and D_t) of 0.27 s and 0.41 s, respectively.

Figures 3.7 and 3.8 show the photocurrent transients for the AlNNW device at 15 V bias under 254nm UV light. The device exhibits a quick response with rise and decay times of 0.27s and 0.41s, respectively, which is faster than the most reported UV photodetectors [37, 38]. The rise time corresponds to the time to reach 90% of its maximum photocurrent value whereas the decay time is the time elapsed for the photocurrent to recover from 90% to 10% of maximum photocurrent. Immediately after the UV illumination is turned OFF, the photocurrent decayed quickly to its dark current values. Moreover during the repeated periodical exposure to UV light, the AlNNW device did not show any persistent photoconductivity (cycles remained similar within the noise level) indicating great reversibility and stability of the device. This high performance not only shows good properties of the AlNNWs, but also quality of the fabrication scheme including the good contacts between the AlNNWs and the Au electrodes.

Compared to other similar studies on flexible nanostructure devices, our present flexible AlNNW UV photodetector exhibits a faster response time. For example, ternary metal oxides Zn_2GeO_4 and $In_2Ge_2O_7$ based flexible photodetectors reports rise time and decay times of 15 s and 1 s, respectively [19] while flexible ZnO nanowire network based UVPD exhibits a 9.1 s and 56 s rise and decay times, respectively [39].

The photodetector was tested under 365 nm UV light, however no significant or stable photocurrent was observed demonstrating the selectivity of our photodetector.

3.3.4 Current Responsivity

Another important performance parameter is the photodetector responsivity, that is the ratio of photocurrent genenrated to the incident energy per effective illuminated area of the photodetector device. The Current responsivity (R_λ) can be calculated by the equation below [40, 41]:

$$R_\lambda = I_\lambda / P_\lambda . A \tag{3.3.2}$$

Where I_λ, P_λ and A are the photocurrent, the light intensity and the effective exposed area, respectively. Based on our experimental results, the responsivity (R_λ) of the AlNNW photodetector is 2.43 mA/W for 254 nm incident wavelength at 15 V.

3.4 Performance comparison with other low-dimensional UV photodetectors

Table 3.1: Performance parameter comparison of our AlNNW device with other nanostructure photodetectors.

Photodetector /Material	UV light (nm)	Bias (V)	Rise time (s)	Decay time (s)	Reference
ZnS nanobelt	300	10	0.3	–	[8]
TiO_2 nanofiber	375	10	~ 2.5	~ 10	[38]
ZnSe nanowire	405	30	0.07	0.2	[42]
Ga_2O_3 nanobelt	250	30	11.8	< 0.3	[22]
AlNNW film	254	1	< 1	< 2	[This work]
AlNNW film	254	15	0.27	0.41	[This work]

Table 3.2: Performance parameter comparison of our AlNNW device with other flexible nanostructure photodetectors.

Photodetector /Flexible substrate	UV light (nm)	Bias (V)	Rise time (s)	Decay time (s)	Reference
Zn_2GeO_4 nanowire	254	20	~ 3	< 1	[19]
$In_2Ge_2O_7$ nanowire	254	20	~ 15	< 1	[19]
ZnO film	385	10	9.1	56	[39]
AlNNW film	254	1	< 1	< 2	[This work]
AlNNW film	254	15	0.27	0.41	[This work]

As summarized in tables 3.1 and 3.2 above, the photoresponse behavior of our AlNNW device is compared to other reported low-dimensional UV photodetectors to to rank its performance. Although our device does not have the fastest time response (among the AlN nanowire based devices), it undeniably offers the following unique advantages: (1) Operation at low bias voltage. Our device can function efficiently and stably as a UV photodetector at low applied voltages as low as 1 V. (2) An inexpensive, simple and practical fabrication method. (3) Relatively quick response and recovery times. Although, the quick response time is very critical for majority of the UV photodetector applications [43], operating voltage is often overlooked limiting their range of application areas. Considering all the above, our devices presents application opportunity in low power consumption ultra-sensitive photonic applications and devices.

Chapter 4

Conclusion and Future Work

4.1 Conclusion

The continuous rapid advancement in fabrication techniques and the growing demand for miniaturized power efficient nanoscale photosensitive devices have driven more studies on various low dimensional semiconductor materials and their geometric structures. One dimensional wide bandgap semiconductor materials due to their excellent electrical and optical properties provide huge potential in fabrication of high sensitivity UV photodetectors.

In my thesis, I have successfully fabricated a very low-cost flexible AlNNWs film based UV photodetector capable of operating at low voltage with good stability and repeatability. Time-dependent dynamics photoresponse behaviour of the device have been studied with varying applied bias voltages ranging from 1 V to 20 V. The photoresponse is a function of bias voltage and an increase in photocurrent is clearly observed with applied voltage. In fact, the photocurrent has increased about seventeen times at 20 V compared to that of at 1 V. In addition to the low voltage operation capability, the device has shown good speed with quick rise and decay times of 0.27 s and 0.41 s, respectively, to the UV illumination. Furthermore, the facile fabrication scheme and good performance opens up new application avenues in low-power consumption sensitive photonic devices as well as wide integration capability with many other flexible and rigid substrates.

In summary, our device offers the following unique advantages:

1. - Operation at low bias voltage. Our device can function efficiently and stably as a UV photodetector at low applied voltages as low as 1 V.
2. - An inexpensive, simple and practical fabrication method.
3. - Relatively quick response and recovery times.
4. - Flexible substrate and light weight UV photodetector.

4.2 Future Work

Despite the considerable progress made in the last few decades there is a lot of room for development in the manufacture of nanoscale UV photodetectors. Challenges such as the synthesis of defect-free nanostructures, the control of their orientations and dimensions still persist, hindering their large scale production and integration. However, as the technology develops, and propelled by the need for portable, light weight, wearable and cost-effective electronic devices, there has been growing research trend flexible electronics. As the field progresses into various applications avenues, it provides interesting opportunity in the development of flexible UVPDs. Still the choice of substrate and integration capability pose a unique challenges. Thus, future works can focus on the different possible choices of substrates (organic or inorganic) compatible with high temperature operation as building blocks for flexible optoelectronic devices.

Bibliography

[1] L. Shi and S. Nihtianov. Comparative study of Silicon-Based Ultraviolet Photodetectors. *IEEE Sens. J. 12*, pages 2453–2459, 2012.

[2] F.R. de Gruijl. Skin cancer and solar UV radiation. *European Journal of Cancer, 35*, pages 2003–2009, 1999.

[3] S. Premi, S. Wallisch, C. M. Mano, A. B. Weiner, A. Bacchiocchi, K. Wakamatsu, E. J. H. Bechara, R. Halaban, T. Douki, and D. E. Brash. Chemical excitation of melanin derivatives induces DNA photoproducts long after UV exposure. *Science 347*, pages 842–847, 2015.

[4] H. Chen, K. Liu, L. Hu, A. A. Al-Ghamdi, and X. Fang. New concept ultraviolet photodetectors. *Mater. Today 18*, pages 493–502, 2015.

[5] Y. Zou, Y. Zhang, Y. Hu, and H. Gu. Ultraviolet Detectors Based on Wide Bandgap Semiconductor Nanowire: A Review. *Sensors 18*, (2072), 2018.

[6] K. Zekentes and K. Rogdakis. SiC nanowires: material and devices. *Journal of Physics D: Applied Physics, 44*, (133001), 2011.

[7] C. Soci, A. Zhang, B. Xiang, S. A. Dayeh, D. P. R. Aplin, J. Park, X. Y. Bao, Y. H. Lo, and D. Wang. ZnO Nanowire UV Photodetectors with High Internal Gain. *Nano. Lett. 7*, pages 1003–1009, 2009.

[8] X. Fang, Y. Bando, M. Liao, U. Gautam, C. Zhi, B. Dierre, B. Liu, T. Zhai, T. Sekiguchi, Y. Koide, and D. Golberg. Single-Crystalline ZnS Nanobelts as Ultraviolet-Light Sensors. *Adv. Mater. 21*, pages 2034–2039, 2009.

[9] L. F. Hu, J. Yan, M. Y. Liao, L. Wu, and X. S. Fang. Ultrahigh External Quantum Efficiency from Thin SnO_2 nanowire Ultraviolet Photodetectors. *Small 7*, pages 1012–1017, 2011.

[10] C. Soci, A. Zhang, B. Xiang, S. A. Dayeh, D. P. R. Aplin, J. Park, X. Y. Bao, Y. H. Lo, and D. Wang. 4H−SiC Ultraviolet avalanche photodetectors with low breakdown voltage and high gain. *Solid-State Electron. 53*, pages 7–10, 2009.

[11] T. Oshima, T. Okuno, N. Arai, N. Suzuki, Sh. Ohira, and Sh. Fujita. Vertical Solar-Blind Deep-Ultraviolet Schottky Photodetectors Based on $\beta - Ga_2O_3$ substrates. *Appl. Phys. Express 1*, (011202), 2008.

[12] R. Suzuki, S. Nakagomi, and Y. Kokubun. Solar-blind photodiodes composed of a Au Schottky contact and a $\beta - Ga_2O_3$ single crystal with a high resistivity cap layer. *Appl. Phys. Lett. 98*, (131114), 2011.

[13] F. González-Posada, R. Songmuang, M. Den Hertog, and E. Monroy. Room-Temperature Photodetection Dynamics of Single GaN Nanowires. *Nano. Lett. 12*, pages 172–176, 2012.

[14] R. F. Davis. III-V nitrides for electronic and optoelectronic applications. pages 702–712, 1991.

[15] S. Y. Wu, H. X. Liu, L. Gu, R. K. Singh, L. Budd, M. Van Schifgaarde, M. R. McCartney, D. J. Smith, and N. Newman. characterization, and modeling of high quality ferromagnetic cr−doped AlN thin film. *Appl. Phys. Lett. 82*, (3047), 2003.

[16] J. Zheng, Y. Yang, B. Yu, X. Song, and X. Li. [0001] Oriented Aluminum Nitride One-Dimensional Nanostructures: Synthesis, Structure Evolution, and Electrical Properties. *ACS Nano 2*, pages 134–142, 2008.

[17] F. Liu, L. Li, T. Guo, H. Gan, X. Mo, J. Chen, S. Deng, and N. Xu. Investigation on the photoconductive behaviors of an individual AlN nanowire under different excited lights. *Nanoscale Res. Lett. 7*, (454), 2012.

[18] Y. B. Tang, X. H. Bo, J. Xu, Y. L. Cao, Z. H. Chen, H. S. Song, C. P. Liu, T. F. Hung, W. J. Zhang, H. M. Cheng, I. Bello, S. T Lee, and C. S. Lee. Tunable p-type conductivity and transport properties of AlN nanowires via Mg doping. *ACS Nano 5*, pages 3591–3598, 2011.

[19] Z. Liu, H. Huang, B. Liang, X. Wang, Z. Wang, D. Chen, and G. Shen. Zn_2GeO_4 and $In_2Ge_2O_7$ nanowire mats based ultraviolet photodetectors on rigid and flexible substrates. *Optics Express 20*, pages 2982–2991, 2012.

[20] Z. Li, F. Li, J. Hu, W. H. Wee, Y. L. Han, B. Pingguan−Murphy, T. J. Lu, and F. Xu. Direct writing electrodes using a ball pen for paper-based point-of-care testing. *Analyst 140*, pages 5526–5535, 2015.

[21] A. R. Madaria, A. Kumar, F. N. Ishikawa, and C. Zhou. highly conductive, and patterned transparent films of a percolating silver nanowire network on rigid and flexible substrates using a dry transfer technique. *Nano Research 3*, pages 564–573, 2010.

[22] L. Li, E. Auer, M. Liao, X. Fang, T. Zhai, U. K. Gautam, A. Lugstein, Y. Koide, Y. Bando, and D. Golberg. Deep−ultraviolet solar-blind photoconductivity of individual gallium oxide nanobelts. *Nanoscale 3*, pages 1120–1126, 2011.

[23] R. H. Yao, J. C. She, Xu N. S., Deng S. Z., and Chen J. Self−assembly of Au−Ag alloy nanoparticles by thermal annealing. *Nanosci. Nanotechnol. 8*, pages 3487–3492, 2008.

[24] M. Jung, K. Y. Eun, J. K. Lee, Y. J. Baik, K. R. Lee, and J. W. Park. Growth of carbon nanotubes by chemical vapor deposition. *Diamond Relat. Mater. 10*, pages 1235–1240, 2001.

[25] https://myscope.training/.

[26] https://www.nanophoton.net.

[27] M. Kuball, J. M. Hayes, A. D. Prins, N. W. A. van Uden, D. J. Dunstan, Y. Shi, and J. H. Edgar. Raman scattering studies on single−crystalline bulk AlN under high pressures. *Appl. Phys. Lett. 78*, (724), 2001.

[28] C. Soci, A. Zhang, X. Y. Bao, H. Kim, Y. Lo, and D. Wang. Nanowire photodetectors. *J Nanosci Nanotechnol. 10*, pages 1430–1449, 2010.

[29] L. Liao, B. Yan, Y. F. Hao, G. Z. Xing, J. P. Liu, B. C. Zhao, Z. X. Shen, T. Wu, L. Wang, and J. T. L. Thong. P−type electrical, Photoconductive, and Anomalous Ferromagnetic properties of Cu_2O Nanowires. *Appl. Phys. Lett. 94*, (113106), 2009.

[30] J. D. Prades, R. Jimenez-Diaz, F. Hernandez-Ramirez, L. Fermandez-Romero, T. Andreu, A. Cirera, A. Romano Rodriguez, A. Cornet, J. R. Morante, and S. Barth. Toward a Systematic Understanding of Photodetectors Based on Individual Metal Oxide Nanowires. *J. Phys. Chem. C 112*, (14639), 2008.

[31] H. M. Huang, R. S. Chen, Chen H. Y., T. W. Liu, C. C. Kuo, C. P. Chen, H. C. Hsu, L. C. Chen, K. H. Chen, and Y. J. Yang. Photoconductivity in single AlN nanowires. *Appl. Phys. Lett. 96*, (062104), 2010.

[32] C. Soci, A. Zhang, B. Xiang, S. A. Dayeh, D. P. R. Aplin, J. Park, X. Y. Bao, Y. H. Lo, and D. Wang. ZnO Nanowire UV Photodetectors with High Internal Gain. *Nano Lett. 7*, pages 1003–1009, 2007.

[33] K. Huang and Q. Zhang. Giant persistent photoconductivity of the WO_3 nanowires in vacuum condition. *Nanoscale Res. Lett. 6*, pages 52–56, 2011.

[34] O. Lopez-Sanchez, D. Lembke, M. Kayci, A. Radenovic, and A. Kis. Ultrasensitive photodetectors based on monolayer MoS_2. *Nat. Nanotech. 8*, pages 497–501, 2013.

[35] A. Sharma, B. Bhattacharyya, A. K. Srivastava, T. D. Senguttuvan, and S. Husale. High performance broadband photodetector using fabricated nanowires of bismuth selenide. *Sci. Rep. 6*, (19138), 2013.

[36] R. Calarco, M. Marso, T. Richter, A. I. Aykanat, R. Meijers, A. V. Hart, T. Stoica, and H. Luth. Size-dependent photoconductivity in MBE-grown GaN nanowires. *Nano Lett. 5*, pages 981–984, 2005.

[37] M. Meng, X. Wu, X. Ji, Z. Gan, L. Liu, and P. K. Shen, J. Chu. Ultrahigh quantum efficiency photodetector and ultrafast reversible surface wettability transition of square In_2O_3 nanowires. *Nano Res. 10*, pages 2772–2781, 2017.

[38] A. J. Molina-Mendiza, A. Moya, R. Frisenda, S. A. Svatek, P. Gant, S. Gonzalez-Abad, E. Antolin, N. Agraït, G. Rubio-Bollinger, and D. P. de Lara. Highly responsive UV-photodetectors based on single electrospun TiO_2 nanofibres. *J. Mater. Chem. C 4*, pages 10707–10714, 2016.

[39] J. Park, J. Lee, Y. Noh, K. Shin, and D. Lee. Flexible ultraviolet photodetectors with ZnO nanowire networks fabricated by large area controlled roll-to-roll processing. *J. Mater. Chem. C 4*, pages 7948–7958, 2016.

[40] J. P. Cheng, Y. J. Zhang, and R. Y. Guo. ZnO Microtube Ultraviolet Detectors. *J. Cryst. Growth 310*, pages 57–61, 2008.

[41] T. Ueda, Z. H. An, K. Hirakawa, and S. Komiyama. Charge-sensitive infrared phototransistors: Characterization by an all−cryogenic spectrometer. *J. Appl. Phys. 103*, (093109), 2008.

[42] E. Oksenberg, R. Popovitz-Biro, K. Rechav, and E. Joselevich. Guided Growth of Horizontal ZnSe Nanowires and their Integration into High−Performance Blue−UV Photodetectors. *Adv. Mater. 27*, pages 3999–4005, 2015.

[43] E. Munoz, E. Monroy, J. L. Pau, F. Calle, F. Omnes, and P. Gibart. III Nitrides and UV Detection. *J. Phys. Cond. Matter 13*, pages 7115–7137, 2001.